GEORG-AUGUST-UNIVERSITÄT
GÖTTINGEN

Fakultät für
Physik

Bachelors Thesis

Ein numerisches Modell für Fluss durch Erdreich

A simple computational model for flow through soil

prepared by

Hannes Hornischer

from Peine

at the Max Planck Institute for Dynamics and Self-Organization

Thesis period: 15th May 2011 until 2nd September 2011

First referee: Prof. Dr. Jürgen Vollmer

Second referee: Prof. Dr. Reiner Kree

Contents

1. Introduction **1**

2. The discrete model and its continuum limit **3**

2.1. Biased random walk model 3

2.2. Continuum limit: BURGERS equation 6

3. Transients **9**

3.1. Constant influx 9

3.1.1. Diffusive decay regime 9

3.1.2. Advectively unstable regime 13

3.1.3. Purely unstable regime 16

3.1.4. Unstable ballistic regime 18

3.1.5. Ballistic regime 19

3.1.6. Discussion 22

3.2. Noisy influx 24

3.2.1. Impact on transients 24

3.2.2. Growth of peaks 26

3.2.3. Discussion 27

4. Steady state regimes **29**

4.1. Deterministic influx 29

4.2. Analytical approach to equilibrium states of the diffusive decay regime 32

4.3. Discussion 35

5. Non-equilibrium phase transitions **37**

5.1. Introduction of cdfs 37

5.2. Introduction to cdfwidth plots 40

5.3. Phase diagrams for constant influx 43

5.4. Phase diagrams for noisy influx 47

5.5. Discussion 50

6. Conclusion & Outlook **53**

A. Numerical algorithm **57**

1. Introduction

To observe flow through porous materials like sand or soil, we can go to small scales and watch water pour out of a flower pot, as well as large scales and analyze the water-level of rivers depending on the precipitation in the catchment area [6]. If we observe a small scale sample, the flower pot, then we see the water flowing quickly out of the pot for dry soil, whereas the water flows slowly for wet soil. So even by watering plants we can determine a nonlinear permeability and a high dependence of the flux on the initial state of a system.
On large scales the behaviour of fluid in soil can be considered as being different. For little water we can assume capillarity to have the greatest impact on flux, whilst for a larger amount of water gravity starts to dominate.
It is quite easy to determine the influx and the resulting outflux, whereas the intermediate evolution of the fluid is tricky. After all, the behaviour of fluid in soil depends on the spatial distribution of fluid content. But how exactly does the flow depend on the initial condition? And also, how does fluid itself evolve?
The transport mechanism of water can be attributed to a diffusive and an advective flux, the latter being in general a function of the spatial distribution of water content. The one-dimensional Burgers equation [7] could therefore be considered the simplest nonlinear continuum-scale model to describe the spatial and temporal evolution of water content in soil. Analytical solutions to the Burgers equation with deterministic boundary conditions were derived in a number of works [7],[1], in particular by Arthur Wachtel in his bachelors thesis preceding the present work [5]. Still, precipitation patterns [3] and the initial distribution of water content [2] themselves are affected by uncertainty. So how do random fluctuations change the behaviour of a system compared to deterministic conditions?

In the present work, we numerically analyze the impact of noise in the boundary terms and uncertainty of initial conditions on the water content distribution. To this end we model the flow by a biased random walk which represents the spatial

and temporal evolution of water density. The soil is modeled as a one-dimensional lattice where the jumping probabilities depend on the local density.
In section 2, we introduce the random walk to model the transport processes and point out that its continuum limit corresponds to the BURGERS equation. In section 3, the transients of certain initial distributions are analyzed in order to learn about how the fluid evolves over time. Also the impact of random noise in the influx on the evolution is discussed. In section 4 we take a look at the steady states and their stability for systems with constant influx. Analysis and discussion of phase spaces are presented in section 5, where we focus on determining the parameters which lead to certain evolution of density distributions.

2. The discrete model and its continuum limit

Since soil is considered a porous material, there exist small hollows which can reasonably be described as a network of interconnected cells. In idealizing the flow through soil as a quasi-one-dimensional process we model this transport process as a biased random walk on a one-dimensional lattice with cells connected by state-dependent jump probabilities. In our model, we consider only jumps to adjacent cells.

2.1. Biased random walk model

The soil is modeled as a one-dimensional lattice with $m+1$ cells with lattice constant a (see Fig. 2.1). At time-step t, each cell i with $i \in \{0, ..., m\}$ contains an amount of fluid $\rho_{i,t}$.

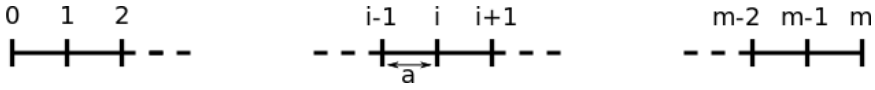

Figure 2.1.: Sketch of an $m+1$ cell model of a soil column.

After each discrete time-step τ a certain amount of fluid moves to the neighboring cells and the rest stays. Consequently, the equation describing the time evolution of the density $\rho_{i,t}$ at node i is given by

$$\rho_{i,t+1} = \underbrace{r_{i-1,t} \cdot \rho_{i-1,t}}_{\text{right}} + \underbrace{l_{i+1,t} \cdot \rho_{i+1,t}}_{\text{left}} + \underbrace{s_{i,t} \cdot \rho_{i,t}}_{\text{stay}} \quad \text{, with } t \in \mathbb{N} \text{ , } i \in \{0, .., m\} \tag{2.1}$$

where $r_{i-1,t}$, $l_{i+1,t}$ and $s_{i,t}$ are the probabilities to jump to the right (from $i-1$ to i), to the left (from $i+1$ to i) and to stay at node i, respectively. Conservation of mass,

is expressed by the condition $s_{i,t} + r_{i,t} + l_{i,t} = 1$. It imposes that $s_{i,t}$ is constant and equal to

$$s_{i,t} = 1 - r_{i,t} - l_{i,t} \quad . \tag{2.2}$$

Using Eqs. (2.1) and (2.2) we can now conclude:

$$\begin{aligned} \rho_{i,t+1} =& r_{i-1,t}\rho_{i-1,t} + l_{i+1,t} \cdot \rho_{i+1,t} + (1 - r_{i,t} - l_{i,t}) \cdot \rho_{i,t} && (2.3)\\ =& \rho_{i,t} + (r_{i-1,t}\rho_{i-1,t} - l_{i,t}\rho_{i,t}) - (r_{i,t}\rho_{i,t} - l_{i+1,t}\rho_{i+1,t}) && (2.4)\\ \Leftrightarrow \frac{\rho_{i,t+1} - \rho_{i,t}}{\tau} =& \frac{\frac{a}{\tau}(r_{i-1,t}\rho_{i-1,t} - l_{i,t}\rho_{i,t}) - \frac{a}{\tau}(r_{i,t}\rho_{i,t} - l_{i+1,t}\rho_{i+1,t})}{a} \quad . && (2.5) \end{aligned}$$

where we introduce the current

$$j_{i+\frac{1}{2},t} = \frac{a}{\tau}(r_{i,t}\rho_{i,t} - l_{i+1,t}\rho_{i+1,t}) \tag{2.6}$$

in order to obtain

$$\frac{\rho_{i,t+1} - \rho_{i,t}}{\tau} = -\frac{j_{i-\frac{1}{2},t} - j_{i+\frac{1}{2},t}}{a} \quad . \tag{2.7}$$

Note that a temporal and spatial dependence of the jump probabilities does not affect these expressions. For soil, the probabilities are in general functions of $\rho_{i,t}$. In the simplest setting they may be defined as follows[1]:

$$\begin{aligned} r_{i,t} =& g + \alpha \cdot \rho_{i,t} \quad , && (2.9)\\ l_{i,t} =& g - \alpha \cdot \rho_{i,t} \quad , && (2.10)\\ s_{i,t} =& 1 - r_{i,t} - l_{i,t} = 1 - 2g \stackrel{!}{=} s \quad , && (2.11) \end{aligned}$$

with constant average transfer probability g and a coefficient α characterizing the ρ-dependent asymmetry of the flow. In general we choose g and α such that $g \gg \alpha$ in order to obtain a small asymmetry and therefore small advection. The asymmetric

[1] The definition of $l_{i,t}$ comprises a cut-off condition to ensure the non-negativity of the jump probabilities:

$$0 \leq \alpha \cdot \rho_{i,t} \leq g \leq 0.5 \quad \forall\, i, t \; . \tag{2.8}$$

If $\alpha\rho_{i,t} > g$, i.e. $l_i < 0$, the cut-off condition resets $l_i = 0$, thus preventing that the transfer probabilities obtain negative values. In this case $r_{i,t} = 2g$ and $s_{i,t}$ is still given by Eq. (2.11).

jump probabilities provide a net advective flux. For $\alpha = 0$ the process will be purely diffusive, whereas increasing values of α correspond to higher advective velocities to the right. In Fig. 2.2 we see a sketch with denoted jump probabilities.

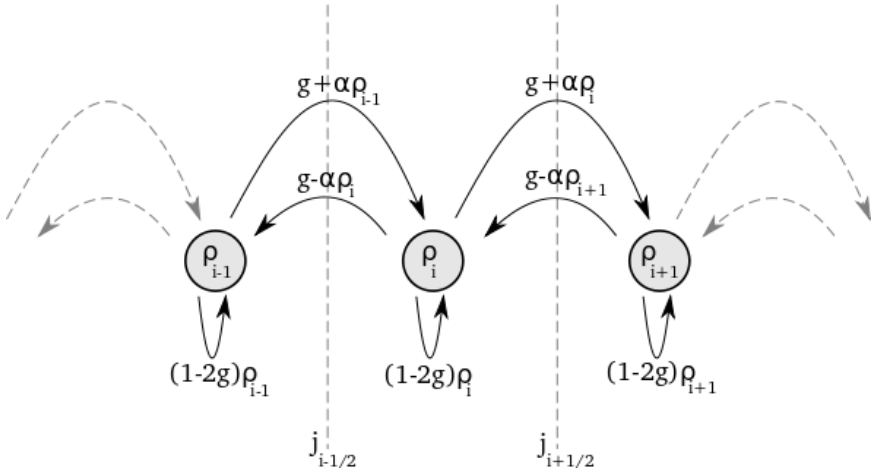

Figure 2.2.: Sketch of the density transfer with denoted densities, jump probabilities and currents.

The equation of motion (2.1) is supplemented by the following initial and boundary conditions:

- The initial condition

$$\rho_{i,0} = Q(x_i) \ , \tag{2.12}$$

  where $Q(x_i)$ is the initial density distribution.

- The inlet boundary condition

$$\rho_{0,t} = A + \gamma W(t) \ , \tag{2.13}$$

  with a constant amplitude A, $W(t)$ a white noise of amplitude 1, and γ a parameter defining the actual amplitude of the white noise. Beside constant influx for $\gamma = 0$ it also allows us to take into account fluctuations of the influx around an average value A.

- The outlet boundary condition

$$\rho_{m,t} = 0 \ , \tag{2.14}$$

simulates matter flowing out of the soil. After all, on the time scale of the diffusive fluxes the effect of a sink at site m will be to instantaneously leading away all water arriving at that point.

2.2. Continuum limit: Burgers equation

We show now that the biased random walk model introduced in the previous section corresponds to the Burgers equation in the continuum limit. Equation (2.7) becomes the continuity equation

$$\frac{\partial \rho(x,t')}{\partial t'} = -\nabla \cdot j(x,t'), \tag{2.15}$$

with $t' = t \cdot \tau$ and $x = (i + \frac{1}{2})a$ as temporal and spatial variables, respectively. The appropriate continuum limit is that for which $\frac{\rho_{i,t} - \rho_{i+1,t}}{a}$ may be written as a derivative of a sufficiently smooth[2] function $\rho(x,t')$ as detailed in [4]. We therefore want to express $j(x,t')$ as a function of $\partial_x \rho(x,t')$. Hence we rewrite Eq. (2.6) in terms of averages and differences,

$$\begin{aligned} j_{i+1/2,t} &= \frac{a}{\tau}(r_i \rho_{i,t} - l_{i+1}\rho_{i+1,t}) \\ &= \frac{a}{\tau}\left(r_i - l_{i+1}\right)\frac{\rho_{i,t} + \rho_{i+1,t}}{2} + \frac{a^2}{\tau}\left(\frac{r_i + l_{i+1}}{2}\right)\frac{\rho_{i,t} - \rho_{i+1,t}}{a} \ . \end{aligned} \tag{2.17}$$

Combining Eq. (2.17) with (2.9) and (2.10) we obtain

$$j_{i+1/2,t} = 2\alpha\frac{a}{\tau}\left(\frac{\rho_{i,t} + \rho_{i+1,t}}{2}\right)\left(\frac{\rho_{i,t} + \rho_{i+1,t}}{2}\right) - \frac{a^2}{\tau}g\left(\frac{\rho_{i+1,t} - \rho_{i,t}}{a}\right) + \frac{a^3}{2\tau}\alpha\left(\frac{\rho_{i+1,t} - \rho_{i,t}}{a}\right)^2 .$$

[2] The condition $\frac{\rho_{i+1,t} - \rho_{i,t}}{a} \to \partial_x \rho(x,t')$ requires sufficiently smooth functions. Here we use

$$\rho^{(n)}(x,t') \gg a\rho^{(n+1)(x,t')} \ , \ \forall n \in \mathbb{N}_0 \tag{2.16}$$

and an analogues condition for $j(x,t')$.

More formally, in the continuum limit $j_{i+1/2,t} \to j(x,t')$ and $\frac{\rho_{i,t}+\rho_{i+1,t}}{2} \to \rho(x,t')$, furthermore, $\frac{\rho_{i+1,t}-\rho_{i,t}}{a} \to \partial_x\rho(x,t')$. Thus, we obtain

$$j(x) = \underbrace{2\alpha\frac{a}{\tau}}_{=:C}\underbrace{\left(\frac{\rho_{i,t}+\rho_{i+1,t}}{2}\right)}_{\to\rho(x,t')}\underbrace{\left(\frac{\rho_{i,t}+\rho_{i+1,t}}{2}\right)}_{\to\rho(x,t')} - \underbrace{g\frac{a^2}{\tau}}_{=:D}\underbrace{\left(\frac{\rho_{i+1,t}-\rho_{i,t}}{a}\right)}_{\to\partial_x\rho(x,t')} + \underbrace{\frac{a^3}{2\tau}\alpha}_{=C\cdot\frac{a^2}{4}}\underbrace{\left(\frac{\rho_{i+1,t}-\rho_{i,t}}{a}\right)^2}_{\to(\partial_x\rho(x,t'))^2} \tag{2.18}$$

$$= C\rho^2(x,t') - D\partial_x\rho(x,t') + a^2\frac{C}{4}(\partial_x\rho(x,t'))^2 \ . \tag{2.19}$$

Eq. (2.16) guarantees

$$a\cdot\partial_x\rho(x,t') \ll \rho(x,t') \tag{2.20}$$

$$\Leftrightarrow \rho_{i+1}-\rho_i \ll \frac{\rho_{i+1}+\rho_i}{2} \quad . \tag{2.21}$$

This holds for all i except right at the absorbing boundary. Thus the last part of Eq. (2.19) becomes

$$a^2\frac{C}{4}(\partial_x\rho(x,t'))^2 = \frac{C}{4}(a\partial_x\rho(x,t'))^2 \ll \frac{C}{4}(\rho(x,t'))^2 \tag{2.22}$$

which is in turn dominated by the first term in Eq. (2.19). For $j(x,t')$ we now have

$$j(x,t') \approx C\rho^2(x,t') - D\partial_x\rho(x,t') \ . \tag{2.23}$$

Combined with Eq. (2.15) this leads to the BURGERS equation

$$\frac{\partial\rho(x,t')}{\partial t'} = -\nabla\cdot j(x,t') = -\frac{\partial}{\partial x}\left[C\rho^2(x,t') - D\partial_x\rho(x,t')\right], \tag{2.24}$$

with $C = 2\alpha a/\tau$ and $D = ga^2/\tau$.

It is worthy of note, that the criterion expressed in Eq. (2.16) is not commensurate with the absorbing boundary condition at the outlet. We would therefore expect deviations from the BURGERS equation solution near the outlet, whose error can be estimated by $a^2\frac{C}{4}(\partial_x\rho(x,t'))^2$. We shall see in later sections, that the solutions to the BURGERS equation are mostly flat for the bulk, and therefore, this error will be of non-negligible magnitude only near the outlet.

Furthermore, we have not incorporated the cut-off (Eq. (2.8)) into the proof above. It therefore stands to reason that the BURGERS equation only applies to those regimes, where the cut-off has no effect.
Given the two limitations detailed above, the most reasonable regime where the BURGERS equation is expected to hold, is the diffusive decay regime. We shall discuss this regime in the upcoming sections.

3. Transients

In this section we address the question of how a given initial density distribution evolves in soil, and to which scale, flower pot or river, our model corresponds. Also we analyze the impact of uncertain precipitation patterns simulated by a random noise in the influx.
We first investigate the transients associated with the solution of the proposed model for deterministic flux boundary conditions at the inlet using $\gamma = 0$ (section 3.1). We take a look at systems with different values of α and g in order to understand their influence on the evolution of the density distribution. Then we change the average density in the system $\overline{\rho}$ and explore the evolution of different initial conditions for a given constant influx $\rho_{0,t}$. By doing this, we will identify five different regimes. At last we analyze the influence of random influx at the evolution by setting $\gamma > 0$ in section 3.2. We assume that precipitation can be modeled as white noise, especially on a very short time scale (hourly or daily), i.e. when seasonal variations can be neglected.

3.1. Constant influx

3.1.1. Diffusive decay regime

We first investigate the impact of α and g on the system's behaviour. Figure 3.1 shows the time evolution of the density from an initial Gaussian distribution for three different values of $\alpha \in \{0, 0.025, 0.05\}$ and a constant $g = 0.4$. The left boundary condition is constant influx, i.e. $\rho_{0,t} = 0.2$.

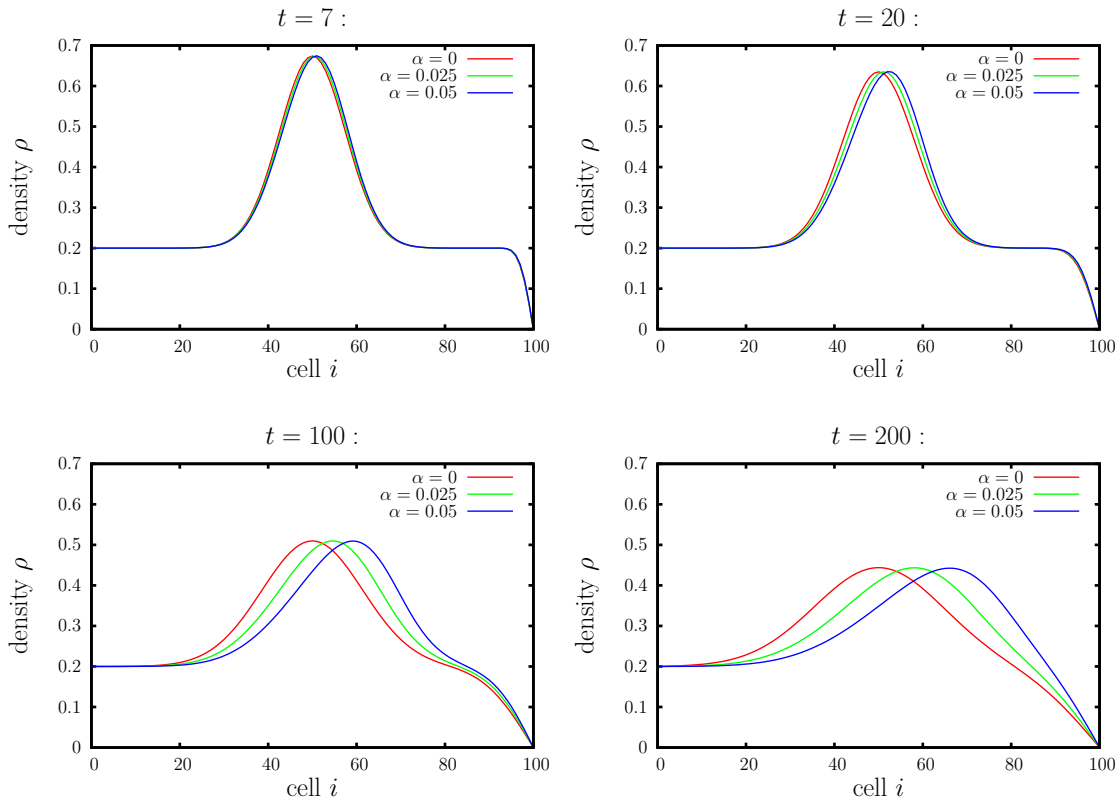

Figure 3.1.: A Gaussian density distribution dissolves, with $\alpha \in \{0, 0.025, 0.05\}$ and $\rho_{0,t} = 0.2$, $g = 0.4$.

Higher values of α correspond to an increased advective effect. This is demonstrated by the location of the density distribution: For $\alpha = 0$ the peak of the curve stays at the same cell whereas for greater values of α the peak propagates to the right. This is consistent with the continuum limit of the biased random walk where the advective coefficient, C, in the BURGERS equation is directly proportional to α.

Figure 3.2 shows the spatial density distribution at four instances in time and three different values of $g \in \{0.2, 0.3, 0.4\}$.

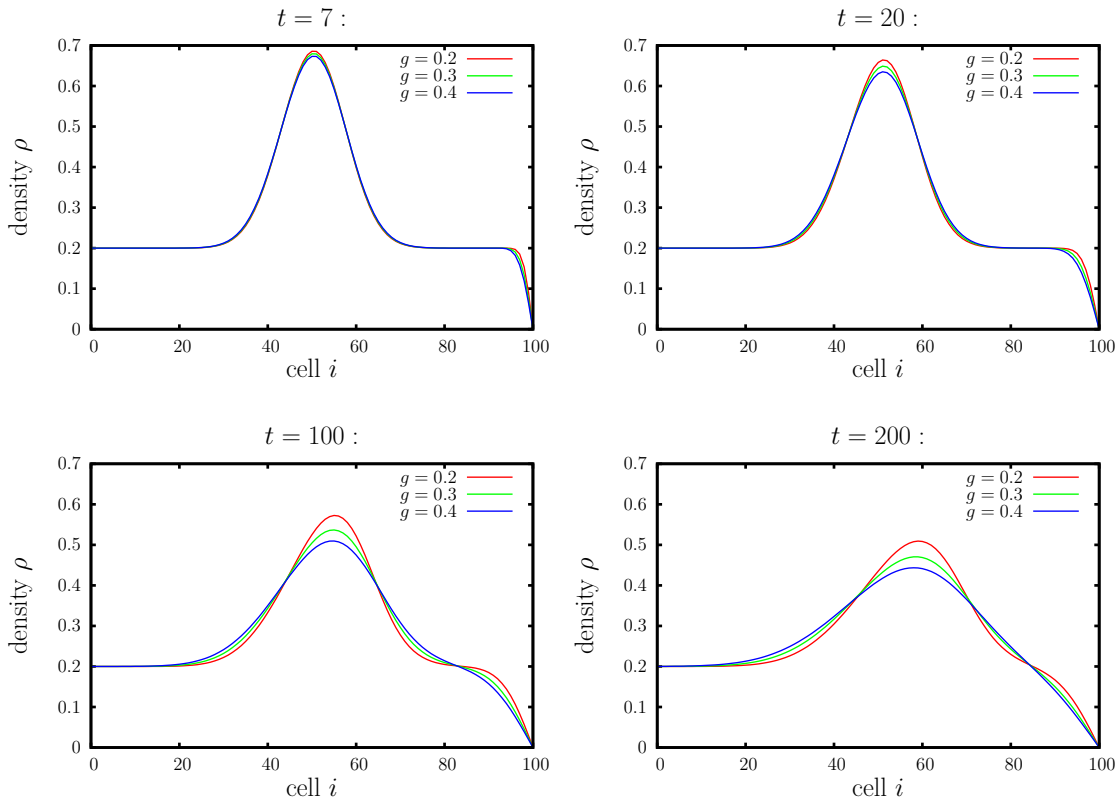

Figure 3.2.: A Gaussian density distribution dissolves, with $g \in \{0.2, 0.3, 0.4\}$ and $\rho_{0,t} = 0.2$, $\alpha = 0.025$.

Again the numerical results are consistent with the theoretical prediction that g is related to the diffusion coefficient D in the continuum limit: the greater g, the more diffusive the system becomes. As expected, the peak of the distribution only mildly moves to the right as the advective contribution is small ($\alpha = 0.025$) compared to the diffusive part. For $g = 0$ nothing would happen, since the probability for a fluid particle to stay at a particular cell i would be $s = 1$ by definition (see Eq. 2.11).

In natural systems, the initial distribution of fluid in the soil is usually unknown or affected by great uncertainty (due to, say, measurement errors or limited sets of data). High fluctuations in initial water content may also be associated with highly heterogeneous materials on a very small spatial scale. We therefore choose a randomly spatially distributed initial density and a random flux density as a boundary condition to the inlet. More specifically, the initial density at each cell is given by a random value, uniformly distributed in an interval centered around an

average density.

Figure 3.3 shows the impact of uncertain initial distribution on the system's evolution. While such uncertainty can lead to unphysical initial distributions of the density (as we face narrow spikes whose occurrence in nature is improbable), however after only few time-steps the spikes smooth out. Also, sharp peaks smooth out much faster compared to more uniformly distributed regions. Large gradients in water content induce a high outgoing flux to neighbouring cells, while experiencing only limited influx. Therefore the greater the gradient, the faster the density differences smooth out. As soon as the density profile is uniform, the influx and outflux at each location tend to counterbalance and density changes slow down.

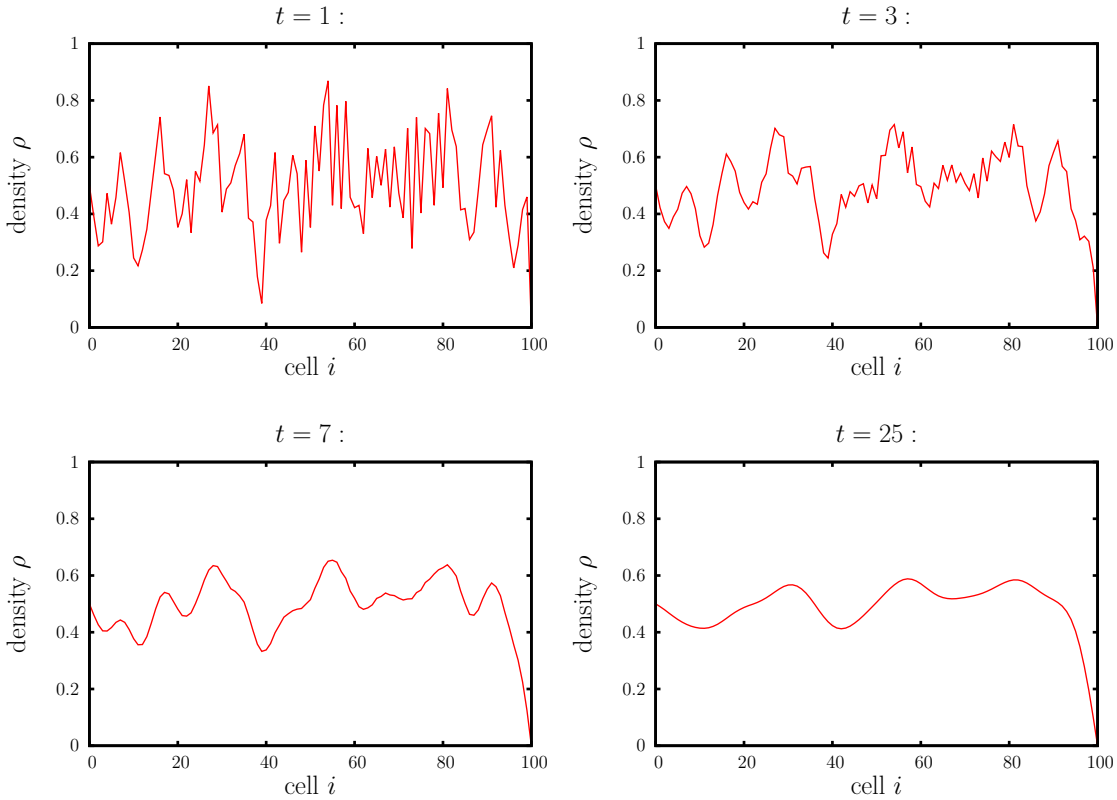

Figure 3.3.: A random density distribution (range 0.5 around average at $\overline{\rho} = 0.5$) dissolves, with $g = 0.4$, $\rho_{0,t} = 0.5$, $\alpha = 0.05$.

3.1.2. Advectively unstable regime

Increasing the average value of the initial distribution changes drastically the system's response. Figure 3.4 shows the spatial density distribution at four different instances in time for a random initial distribution with average value $\overline{\rho} = 5.5$.

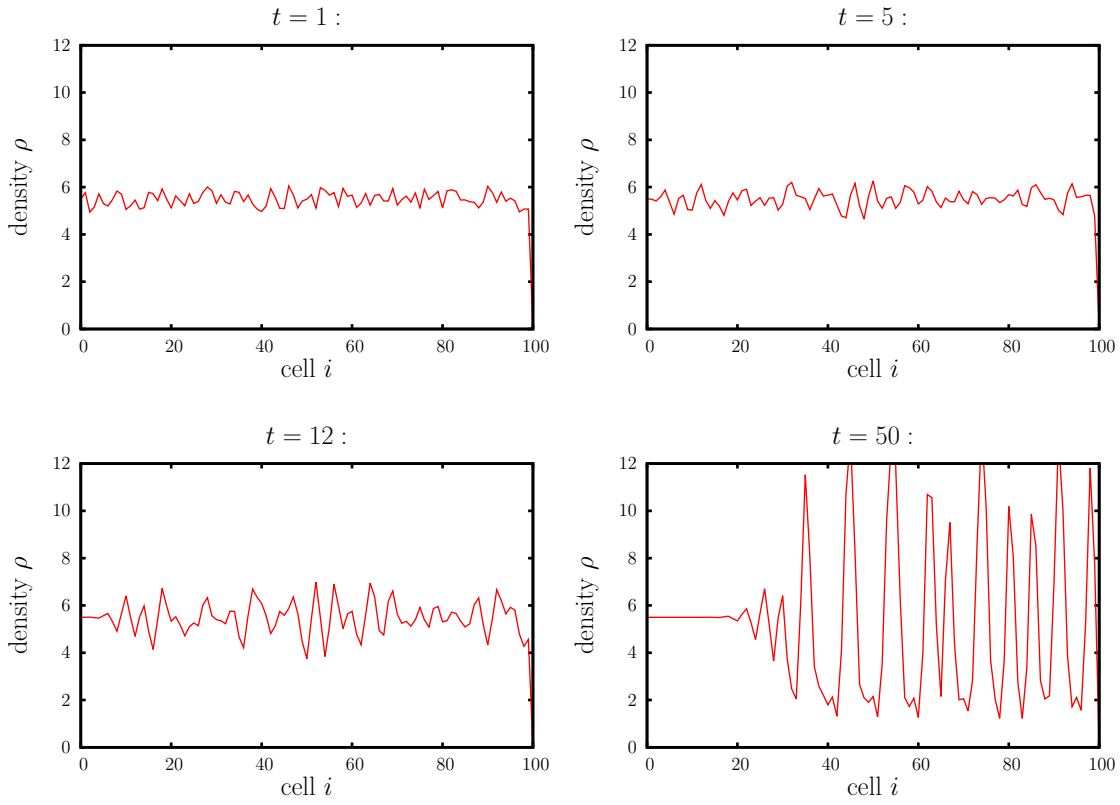

Figure 3.4.: A random density distribution (range 0.5 around average at $\overline{\rho} = 5.5$) dissolves, with $g = 0.4$ and $\rho_{0,t} = 5.5$, $\alpha = 0.05$.

Instead of smoothing out, the density distribution develops a spiky shape with values varying between $\rho_{min} \approx 2$ to $\rho_{max} \approx 12$. Compared to Fig. 3.3 the system is also more advective and a flat line appears on the left hand side of the domain. Since the advective term $\alpha\rho$ in Eqs. (2.9) and (2.10) is proportional to the density, increasing the average value of the overall initial distribution translates to increased advection. This leads to a constant inlet signal that propagates undisturbed.

The lower cut-off around $\rho \approx 2$ results from a constant probability to stay $s_i = 0.2$ (see Eq. (2.11)). Since the density at a peak is around $\rho_{peak} \approx 12$, the probability

for its matter to jump right is around its maximum at $r_i = 0.8$. So when the fluid of a peak jumps right, the fluid left over is around $\rho_{leftover} = s \cdot \rho_{peak} \approx 0.2 \cdot 12 = 2.4$. To better understand the evolution of such peaks, we take a look at a single peak in an otherwise uniform distribution with average density of $\overline{\rho} = 4.8$. Without the peak, the density distribution in that system would be constant in time.

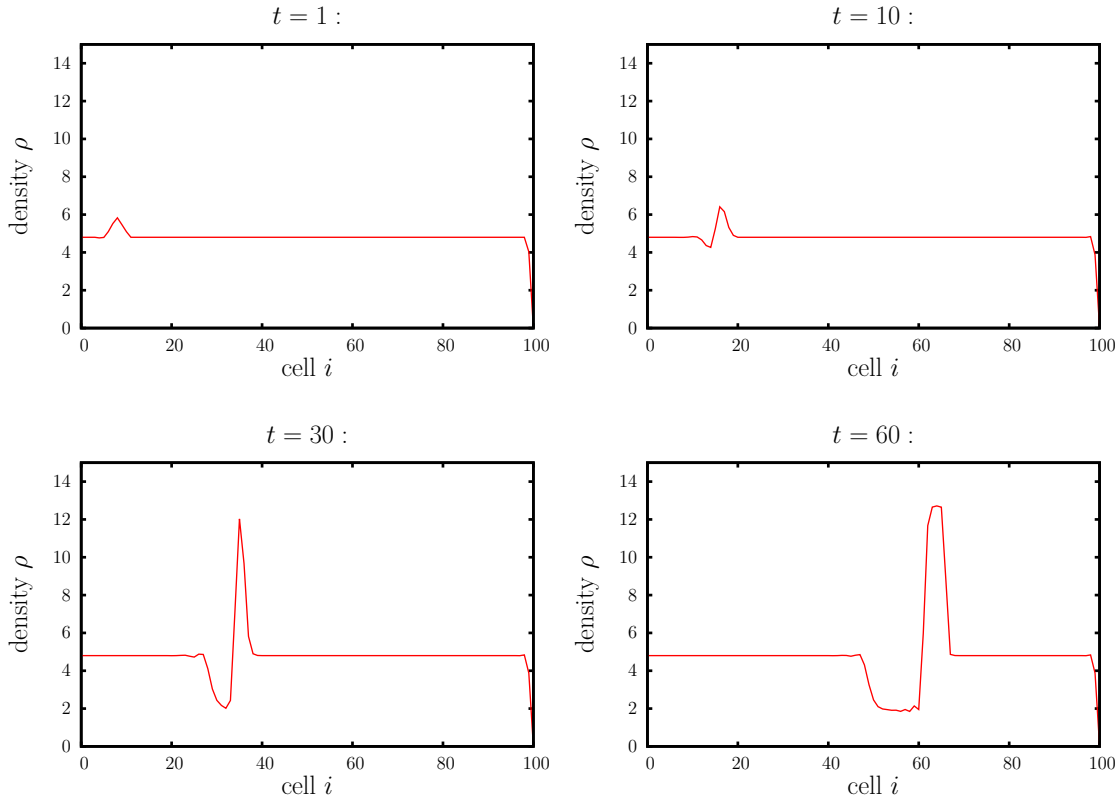

Figure 3.5.: A triangular peak of height 1 above the average density $\overline{\rho} = 4.8$ and width of 5 cells evolving with $g = 0.4$, $\rho_{0,t} = 4.8$, $\alpha = 0.05$.

The peak is moving to the right, growing up to a height of $\rho \approx 12$ and growing constantly in width. At the same time at the left hand side of the peak a depression appears. Its bottom is at $\rho \approx 2$ and it is also constantly growing in width. Also a small hump arises at the left side of the depression.
Due to a higher density, the peak is advecting faster than the unperturbed system around it. This causes the peak to absorb the fluid downstream and thereby it grows. On the other hand the peak leaves behind a depression. The fluid behind the peak advects not fast enough to keep up, thereby allowing the depression to

grow.
The hump emerges from the fluid coming from the inlet summing up with the slower advecting fluid in the depression.
After increasing our average density up to $\overline{\rho} = \rho_{0,t} = 5.5$, another change in the behaviour appears.

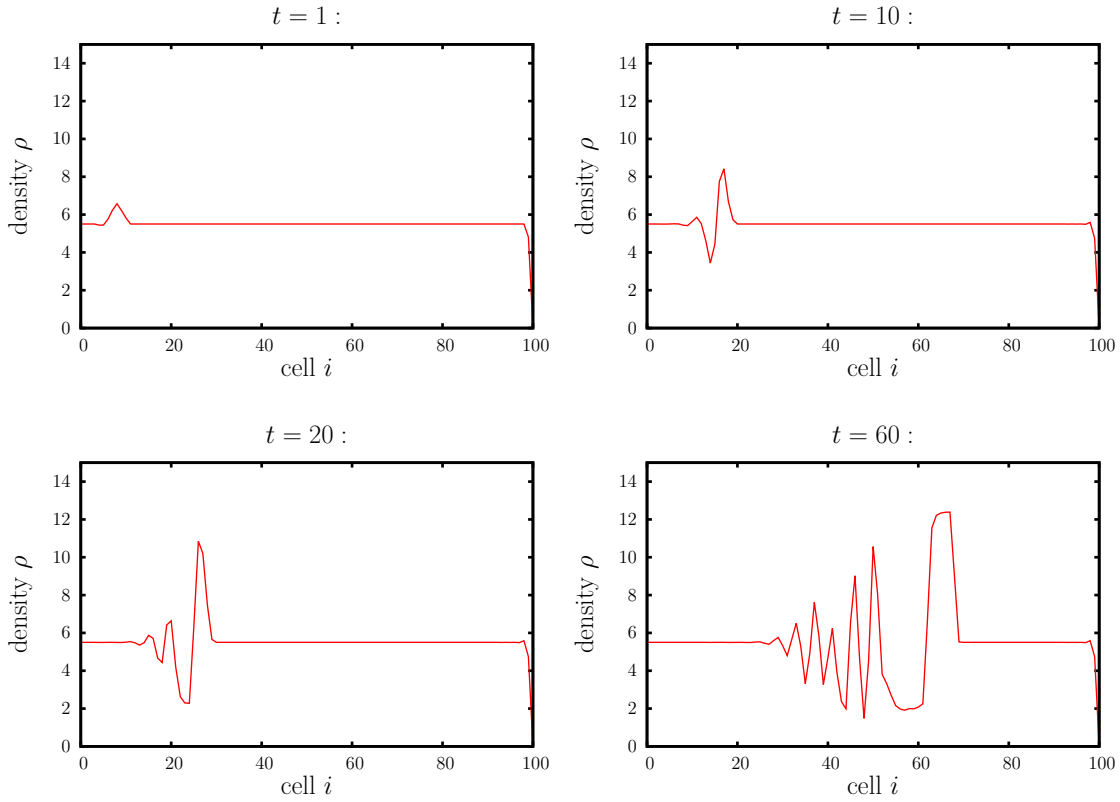

Figure 3.6.: A triangular peak of height 1 above the average density $\overline{\rho} = 5.5$ and width of 5 cells evolving with $g = 0.4$, $\rho_{0,t} = 5.5$, $\alpha = 0.05$.

At the left hand side of the depression spikes appear while otherwise pretty much the same is happening as at the average density $\overline{\rho} = \rho_{0,t} = 4.8$ in Fig. 3.5, only now the system is unstable enough to produce spikes out of the hump left hand side from the depression. The spikes generally show the same behaviour as a single peak, only they do not develop a depression but more spikes instead. Therefore it takes the distribution more time to vanish in the outlet.
We now analyze the connection between the height of the system and the occurrence of these spikes. The following figure shows the same initial distribution as in Fig. 3.5

and 3.6 at different heights of the system right before vanishing in the outlet:

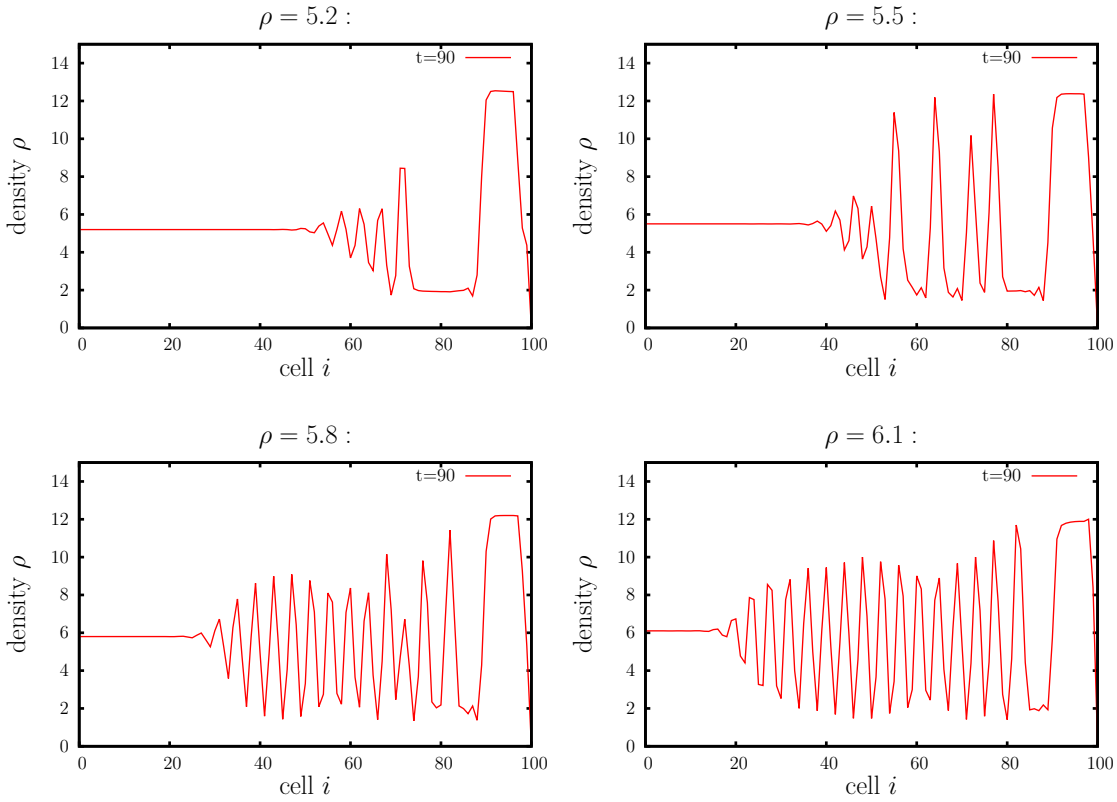

Figure 3.7.: A triangular peak of height 1 above the average density $\overline{\rho} = \rho_{0,t}$ and width of 5 cells at time $t = 90$ right before vanishing for $\rho_{0,t} \in \{5.2, 5.5, 5.8, 6.1\}$ and $g = 0.4$, $\alpha = 0.05$.

For each value of $\overline{\rho}$ the peak reached the outlet at the same time $t = 90$, but for higher values, more spikes appear at the left hand side of the depression. For $\rho_{0,t} = 5.2$ and $\rho_{0,t} = 5.5$ these spikes look quite random, but for $\rho_{0,t} = 5.8$ and $\rho_{0,t} = 6.1$ we recognize an oscillation-like shape. Thus for larger height of the system, more spikes appear and the time until the initial distribution vanishes in the outlet is larger. At a critical $\overline{\rho}$ spikes actually start moving to the left like shown in the following section.

3.1.3. Purely unstable regime

So far, spikes only arose from existing irregularities in the density distribution. For example as shown in Fig. 3.7, for sufficiently large times the initial distribution

always vanished, leaving a uniform distribution with a sink at the outlet. Once spiky structures evolve upstream, no steady, uniform distribution will ever appear. In this regime a random initial distribution would simply look like Fig. 3.4 without the flat line, so without ever vanishing in the outlet. In order to observe spikes evolving upstream we now have a look at a uniform initial distribution at height $\rho = 7.5$ in the following figure.

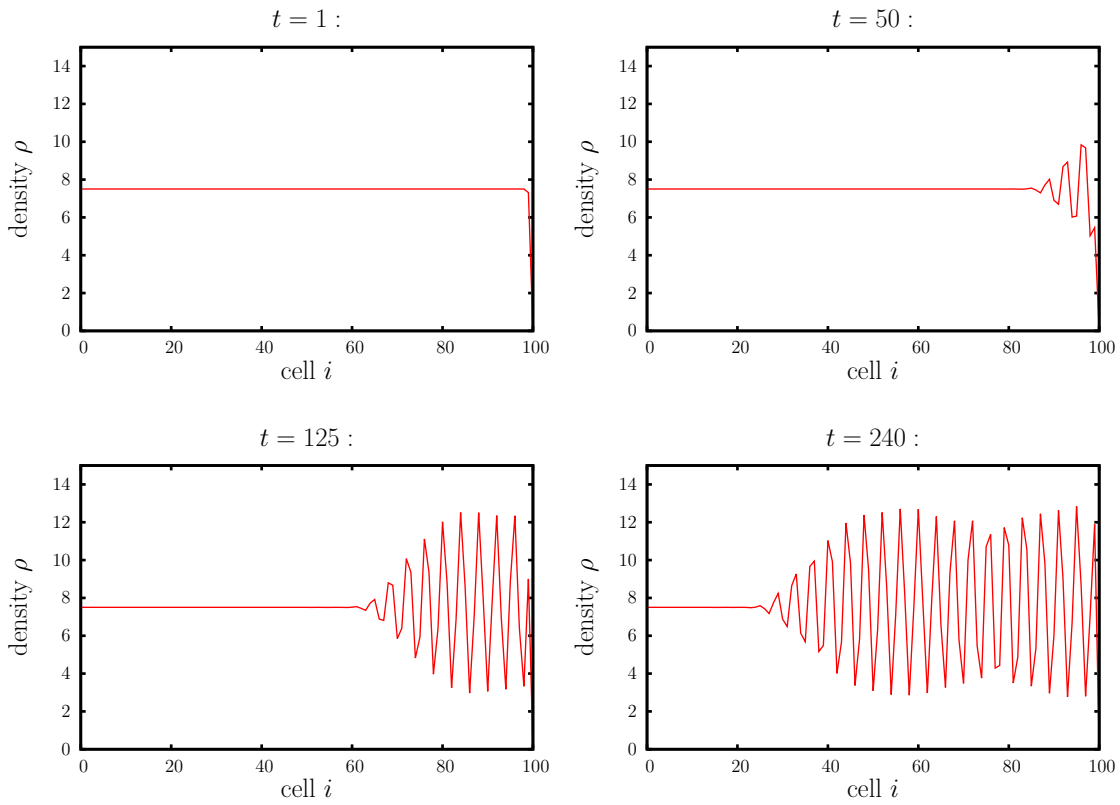

Figure 3.8.: A constant initial distribution at height $\rho_{const} = 7.5$ building up spikes for $g = 0.4$, $\rho_{0,t} = 7.5$, $\alpha = 0.05$.

First some fluctuations at the outlet are visible which then slowly evolve into spikes. The spiky domain spreads out, moving upstream showing an oscillatory structure already observed in Fig. 3.7. What is not clearly visible in this figure, is that the spikes still advect downstream, only the domain containing spikes moves upstream. While spikes still advect downstream, they create small fluctuations to the left from them. These fluctuations grow, advecting downstream also creating fluctuations to the left. In this way, after sufficient time, the whole system is populated with

spikes. Obviously the distribution will never be "washed away" and also never reach an equilibrium state, since the spikes continue moving downstream.

3.1.4. Unstable ballistic regime

Increasing the average value of the initial distribution leads to yet another type of behaviour. We now consider a random initial distribution with average $\overline{\rho} = 9$. The system evolution at four different times is shown in Figure 3.9.

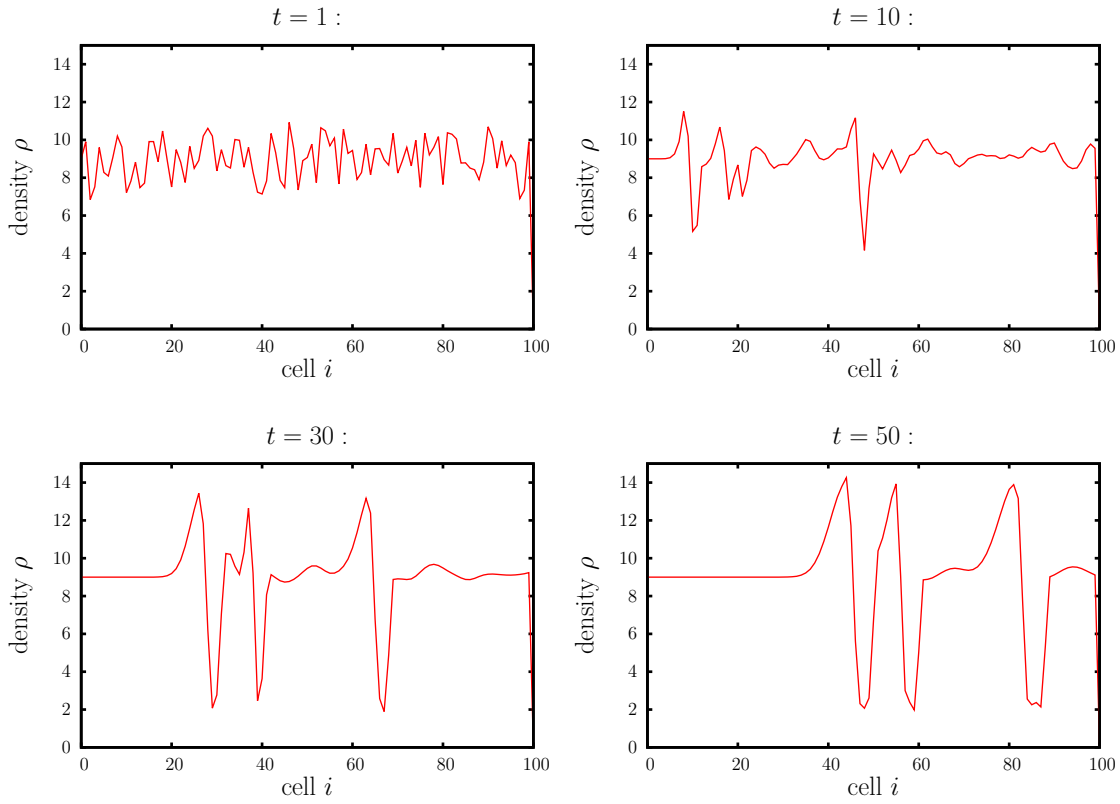

Figure 3.9.: A random density distribution (range 1.0 around average at $\overline{\rho} = 9.0$) dissolves, with $g = 0.4$ and $\rho_{0,t} = 9.0$, $\alpha = 0.05$.

The random initial distribution smooths out in a similar fashion to the one in Fig. 3.3 with the only difference now that the system is more advective. At the same time few single spikes arise, propagating to the right without producing more spikes. This time the depression is on the right of each spike. The whole system is moving

downstream finally vanishing at the outlet. Due to a higher average density and thereby stronger advection (compared to the systems in the previous figures), no more spikes are generated by other spikes. They simply advect quickly downstream. Still some are growing, but different than before, as now the depression is at the right of the peak (for comparison see Fig. 3.5). An area with initially very low density is advecting slightly slower than the fluid left from it and thereby dams up a peak. However, the rest of the distribution is simply diffusing while advecting very quickly to the outlet.

3.1.5. Ballistic regime

The same random distribution with average density at $\overline{\rho} = 10.0$ shows no more spikes (see Fig. 3.10).

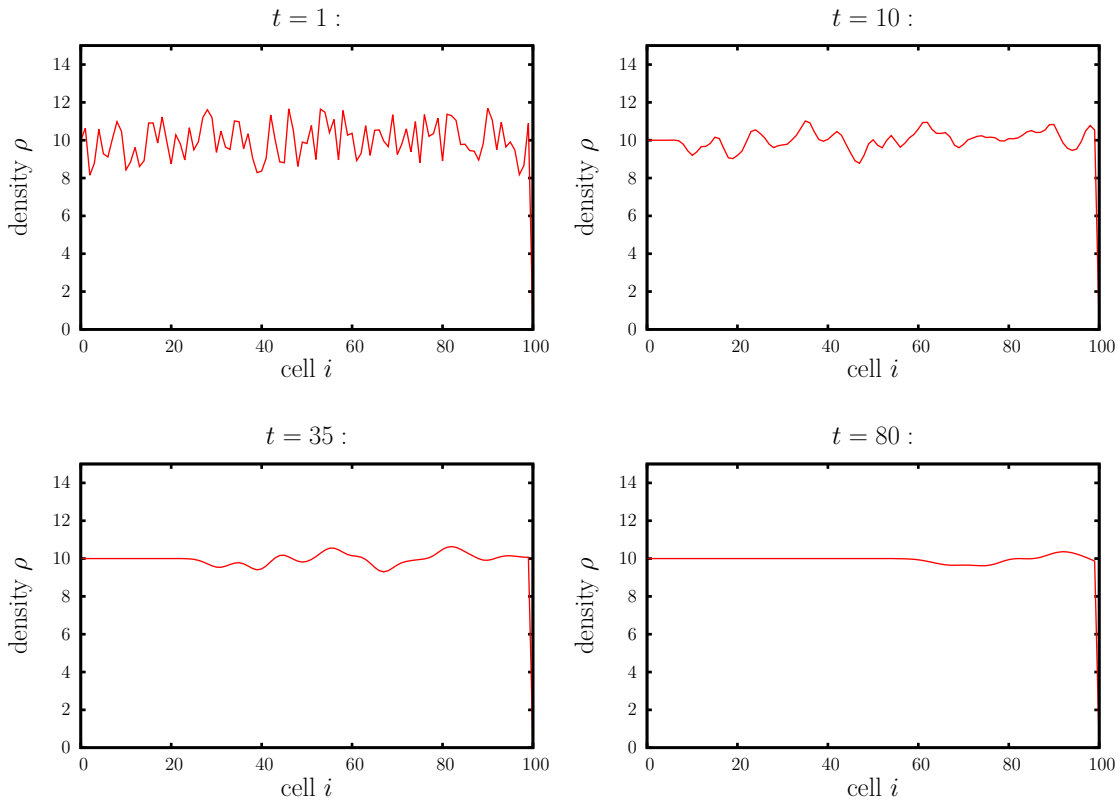

Figure 3.10.: A random density distribution (range 1.0 around average at $\rho = 10.0$) dissolves, with $g = 0.4$ and $\rho_{0,t} = 10.0$, $\alpha = 0.05$.

The random initial distribution smooths out and flows quickly to the right, vanishing

at the outlet. Now the advection is so strong that no spikes can build up and the whole distribution just flows out. The density at every cell is so large that $\alpha\rho \geq 0.4 = g$ and thus the cut-off condition from Eq. (2.8) kicks in. In this case there is no jumping to the left possible anymore and everything is rushing through the system. Hence, the behaviour of a distribution does not change for higher levels of density, like shown in Fig. 3.11.

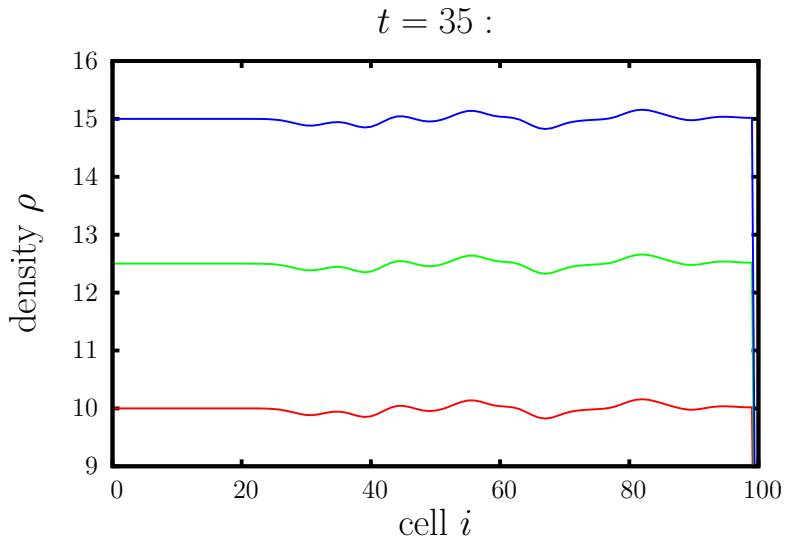

Figure 3.11.: Three random density distribution (range 1.0 around average at $\overline{\rho} \in \{10.0, 12.5, 15.0\}$ dissolving with $g = 0.4$, $\rho_{0,t} = \overline{\rho}$, $\alpha = 0.05$.

We see three identical density distributions at time $t = 35$. Due to the cut-off condition and thereby a fixed probability to jump, the behaviour for different distributions higher than $\overline{\rho} \approx 10$ is identical.
In the following figure we examine the evolution of a single peak in order to analyze the behaviour and compare it to some analytical considerations.

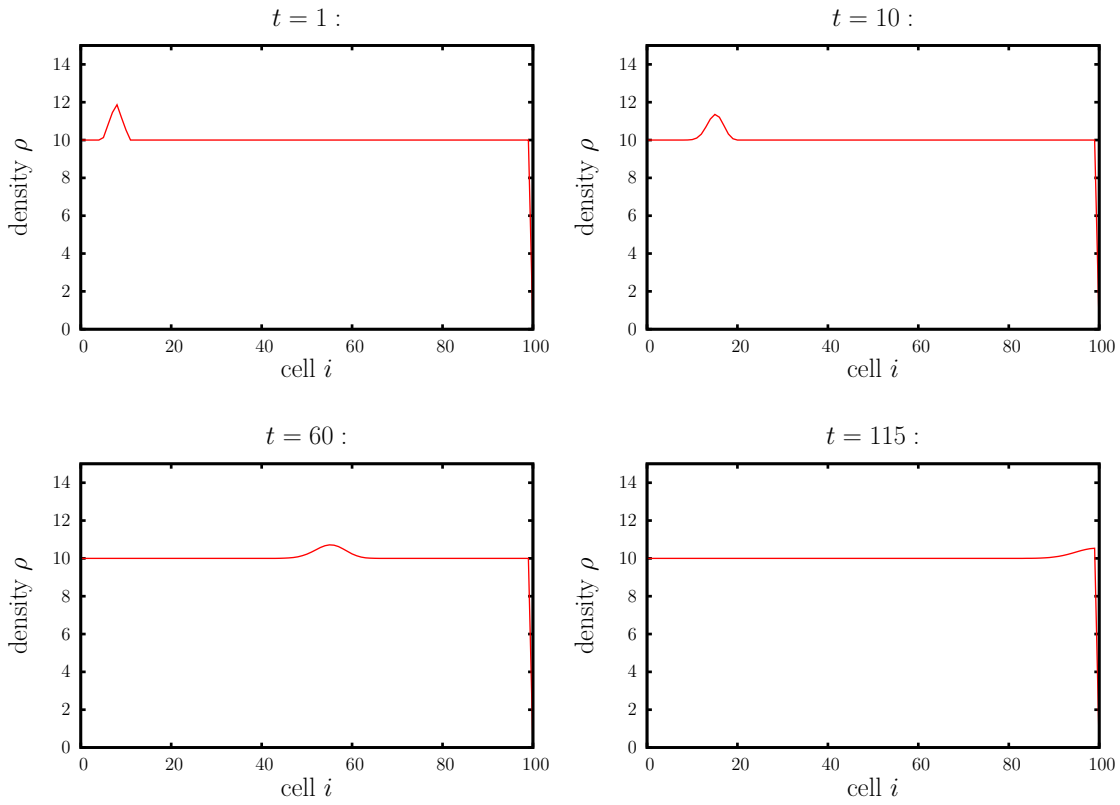

Figure 3.12.: A constant density distribution with a triangular peak of height 2 above the average density and initial width of 5 cells. The peak moves quickly to the outlet at maximum speed of $v = 0.8\frac{a}{\tau}$ due to the probability to jump constantly at $r_i = 0.8$. Parameters: $\rho_{0,t} = 10.0$, $g = 0.4$, $\alpha = 0.05$

The signal with its peak at cell $i = 7$ rushes through the system, diffusing at the same time. Around time $t = 115$ the peak of the distribution is at the last cell $i = 100$. Also it is not dissolving symmetrical. The left slope is longer than the right one. Since we are at such a high density, the peak is moving with maximum speed of $v = 0.8\frac{a}{\tau}$ since the probability to jump right is constantly $r_i = 0.8$. The peak starts at $i = 7$, $t = 0$ and should have covered a distance of $d = 93$ cells after $t_{93cells} = \frac{d}{v} = \frac{93}{0.8} = 116.25$ which fits our observed time.

3.1.6. Discussion

Increasing the average value of the initial density distribution $\overline{\rho}$ leads to five different regimes. We used $g = 0.4$, $\alpha = 0.05$ and $\rho_{0,t} = \overline{\rho}$. Please keep in mind that different sets of parameters would lead to different regimes for constant $\overline{\rho}$. The five regimes are summarized below.

1. $\overline{\rho} \lesssim 3.0$: The **diffusive decay regime** shows a diffusive and slightly advective behaviour of the system (see Fig. 3.3).

2. $3.0 \lesssim \overline{\rho} \lesssim 6.5$: In the **advectively unstable regime** spikes appear. The density distribution does not smooth out. Such spikes grow and advect downstream to the outlet where they vanish, leaving a flat stable density distribution as shown in Fig. 3.4.

3. $6.5 \lesssim \overline{\rho} \lesssim 8.0$: In the **purely unstable regime**, spikes are formed and advect upstream (to the left). In this regime, no steady state can ever be reached since the gradient at the outlet grows to a spike which moves upstream like in Fig. 3.8.

4. $8.0 \lesssim \overline{\rho} \lesssim 9.5$: The **unstable ballistic regime** involves growing peaks as well, but due to a different mechanism. In general the cut-off condition from Eq. (2.8) corresponds to a maximum probability of jumping to the right (downstream) and forbids jumping to the left (upstream). If the density at a cell is small enough for the cut-off condition to not apply, the depression is moving slower than the surrounding. The fluid in the cells downstream of the depression advects faster than the depression itself which therefore broadens. The fluid in the depression jumps partially to the left, creating a peak at the left side like shown in Fig. 3.9.

5. $9.5 \lesssim \overline{\rho}$: In the **ballistic regime** the cut-off condition applies at every cell. The whole system advects downstream at maximum speed while diffusing (see Fig. 3.11).

Also we were able to identify the impact of some parameters of the evolution.

- α in general affects the advection of a system. The greater α, the faster the system flows downstream whereas for $\alpha = 0$ the behaviour is purely diffusive (see Fig. 3.1).

- g determines the diffusive behaviour of a system (Fig. 3.2). After all, the diffusion coefficient $D = g\frac{a^2}{\tau}$ grows with g.
- The initial condition and the influx $\rho_{0,t}$ determine the advective behaviour as well as the regime of the system. For higher density we deal with higher advection since the asymmetric term in the jump probabilities $\pm\alpha\rho$ grows with the density (see Eqs. (2.9), (2.10)).

Since, with higher density we observe higher advection, we could interpret the asymmetric part of the jump probabilities as gravitational force. Thereby our model qualitatively fits the evolution of water flowing from a catchment area to a river corresponding with large scale soil mentioned in the introduction. We also have an impression of how the evolution of water in soil could look like.

3.2. Noisy influx

We now focus on random boundary conditions at the inlet and its development in different regimes. Specifically, we consider the boundary condition (2.13) to be a fluctuating influx with average A and a white noise of amplitude γ around the average value. Also we will analyze the pace at which a peak builds up from a fluctuation.

3.2.1. Impact on transients

First we have a look at the influence of a white noise on a random initial distribution in the diffusive decay regime. Figure 3.13 shows such a system compared to the same system with constant inlet signal.

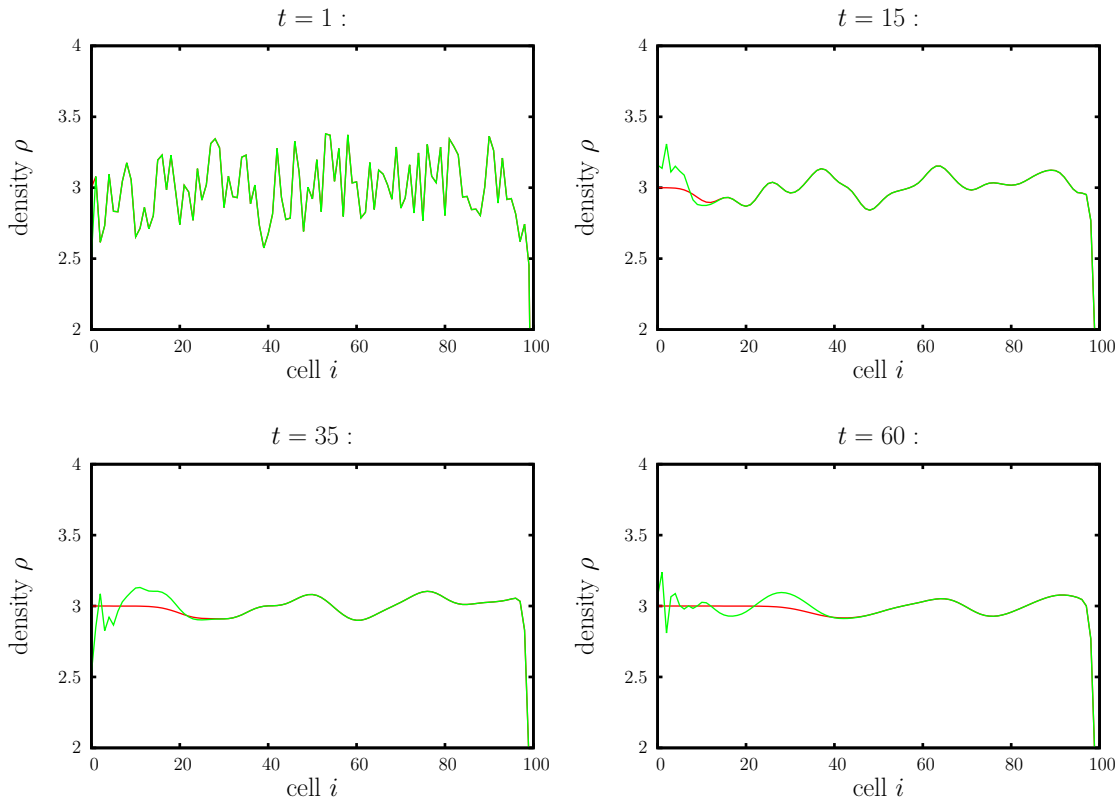

Figure 3.13.: A random initial distribution dissolving with (green curve) and without (red curve) white noise $\gamma = 0.5$, $\gamma = 0.0$ and $g = 0.4$, $\rho_{0,t} = 3.0 + \gamma W(t)$, $\alpha = 0.05$.

At first the distributions are identical. For larger times, more differences arise. The distribution without white noise settles into a constant line at the inlet whereas the one with white noise shows random spikes dissolving to a curve similar to the dissolving initial distribution.
The evolution of a constant initial distribution in the advectively unstable regime is shown in the following figure:

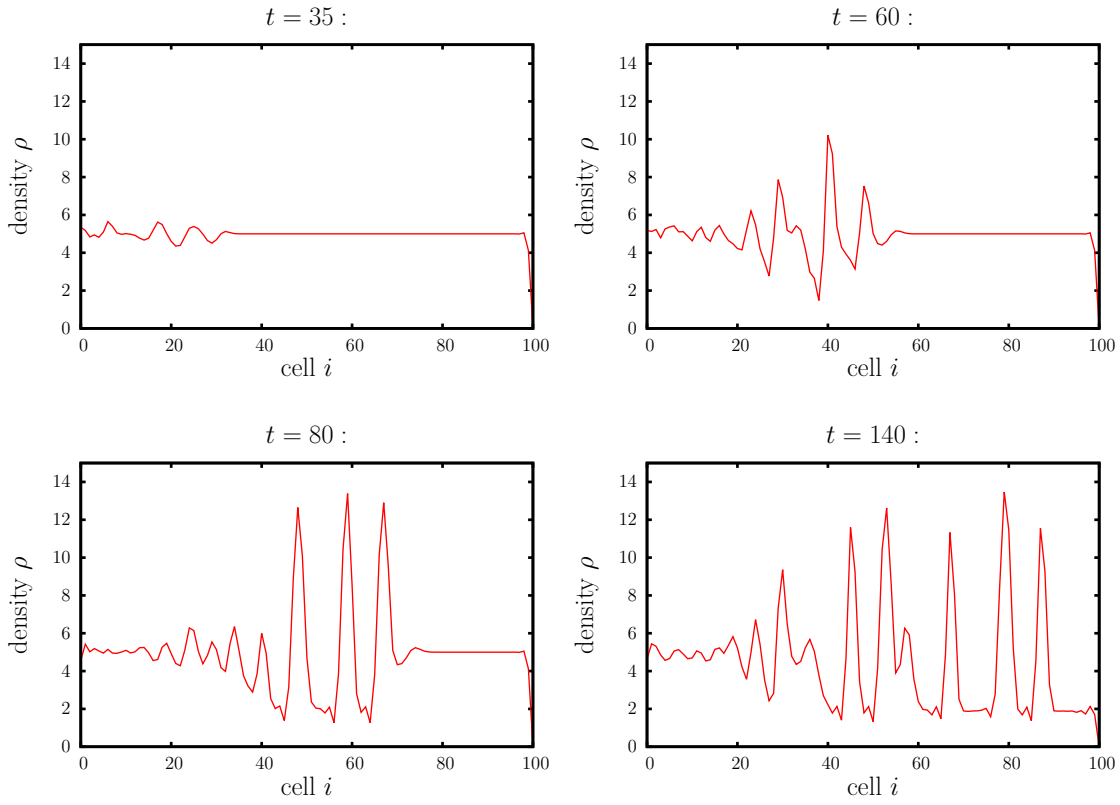

Figure 3.14.: A constant initial distribution with density $\rho_{const} = 5.0$ evolves with white noise $\gamma = 0.5$, $g = 0.4$, $\rho_{0,t} = 5.0 + \gamma W(t)$, $\alpha = 0.05$.

First, some few fluctuations are visible, quickly growing into spikes between $\rho \approx 2$ an $\rho \approx 12$. The random noise produces gradients large enough to grow and show a spiky distribution like in Fig. 3.4.
Concerning the ballistic regime, the white noise has no influence on the initial distribution, since everything is advecting at maximum speed.

3.2.2. Growth of peaks

Since the white noise is a source of random fluctuations in a certain range γ, we can use it to learn about the pace at which a peak grows. The following figure shows a constant initial distribution in the advectively unstable regime with a noisy influx $\rho_{0,t} = 5.0 + 0.1W(t)$. Visible are the densities at each cell for each step over a time-span of $T = 5000\tau$.

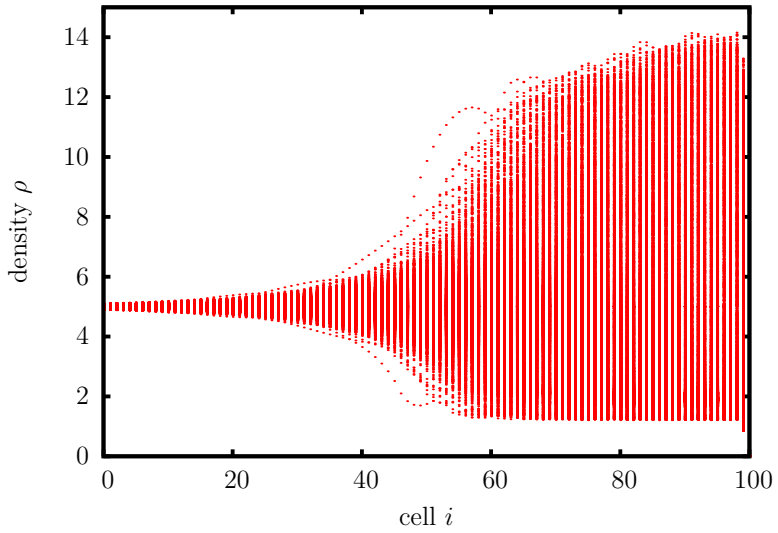

Figure 3.15.: The density of each cell and time-step for a constant initial distribution $\rho_{const} = 5.0$ with white noise of amplitude $\gamma = 0.1$ during 5000 time-steps. Parameters: $g = 0.4$, $\alpha = 0.05$, $\rho_{0,t} = 5.0 + \gamma W(t)$.

We see a cone-shaped distribution of dots which is sharp at the first 20 cells and gets more and more blurry after that. At the last 30 cells it is quite sharp again. We can see in this figure how fast peaks are able to grow in general. In the beginning, all dots are close to each other. Then they grow depending on the initial size of a peak. Since every size of peaks appears with equal likelihood, maximum values are rarely produced. This explains the blurry border from cell $i = 20$ to $i = 80$ where few very large peaks are visible. For the last cells, the maximum is reached since the ballistic regime sets a limit to the growth of peaks.
Obviously, the growing rate of peaks in this model is nonlinear. For peaks with density smaller than $\rho < 10$ we can say for certain, the larger the peak, the faster it grows.

3.2.3. Discussion

In general the transients with white noise in the influx show no conceptionally new aspects of behaviour compared to the deterministic transients. In the diffusive decay regime, peaks due to white noise dissolve very quick. Therefore its influence on the distribution is very small after some time. In the advectively unstable regime it prevents the system from becoming stable while in the purely unstable system it would prevent an oscillatory or generally regular behaviour like the one seen in Fig. 3.8. In the unstable ballistic regime it would constantly create few spikes essentially providing the system with an initial distribution like in Fig. 3.9 at the inlet. In the ballistic regime it just flows through the systems without any effect on the initial distributions.

4. Steady state regimes

A different way to deal with unknown initial distributions of fluid in soil is to concentrate on the boundary signal and wait for the initial distribution to be washed out. Beyond that time the current distribution is determined by the known boundary signals and a known behaviour of the fluid. For a constant inlet signal we will take a look at deterministic systems after a long time, that is to say, at the shape of the equilibrium distributions. First we confirm the independence of an equilibrium distribution on the initial density distribution. After comparing the equilibrium states of each regime, we analytically determine the equilibrium state of the diffusive decay regime and compare it with numerical results.

4.1. Deterministic influx

For a constant inlet signal generally every distribution converges to a steady state if we wait a sufficiently long time. The following figure shows three different initial distributions in the diffusive decay regime with the same constant inlet boundary condition $\rho_{0,t} = 0.5$:

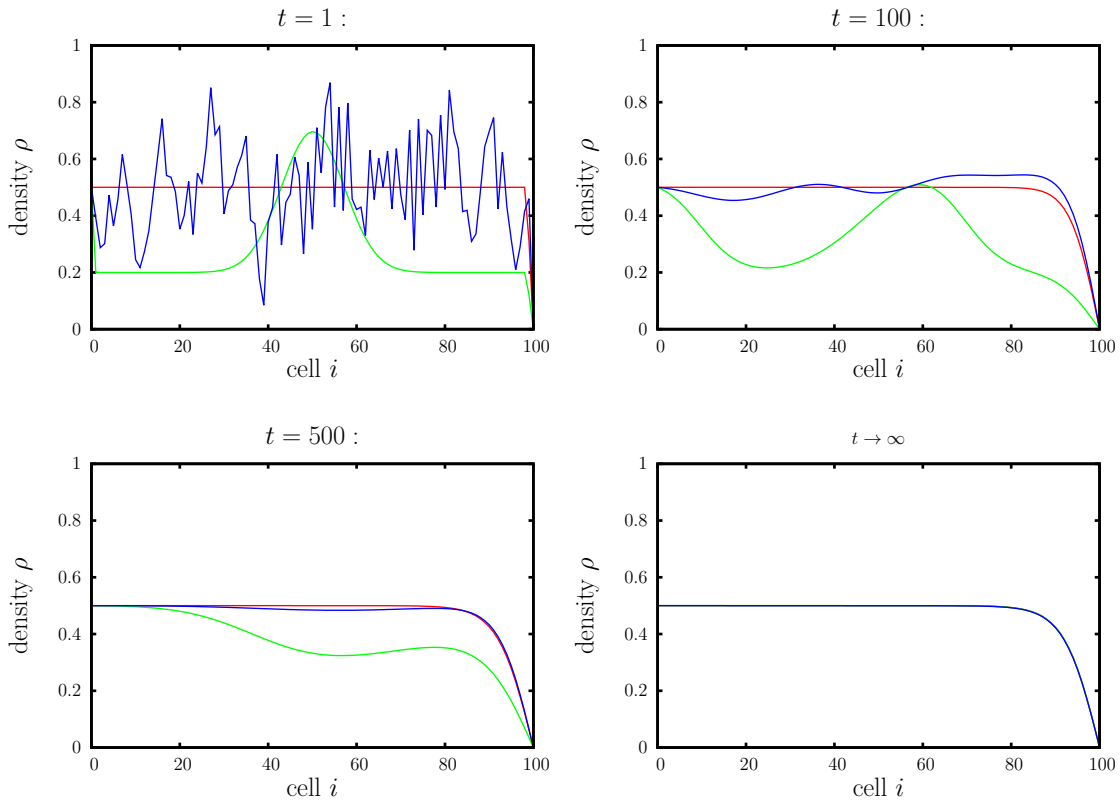

Figure 4.1.: Three different initial distributions (constant distribution with density $\rho_{const} = 0.5$ (red), Gaussian distribution on influx level $\rho = 0.2$ (green), random distribution with range 0.5 around average $\overline{\rho} = 0.5$(blue)) converge to the same equilibrium state with $g = 0.4$, $\rho_{0,t} = 0.5$, $\alpha = 0.05$.

The three initial distributions converge to the same distribution, a steady state. The equilibrium states for the other four regimes look like the following:

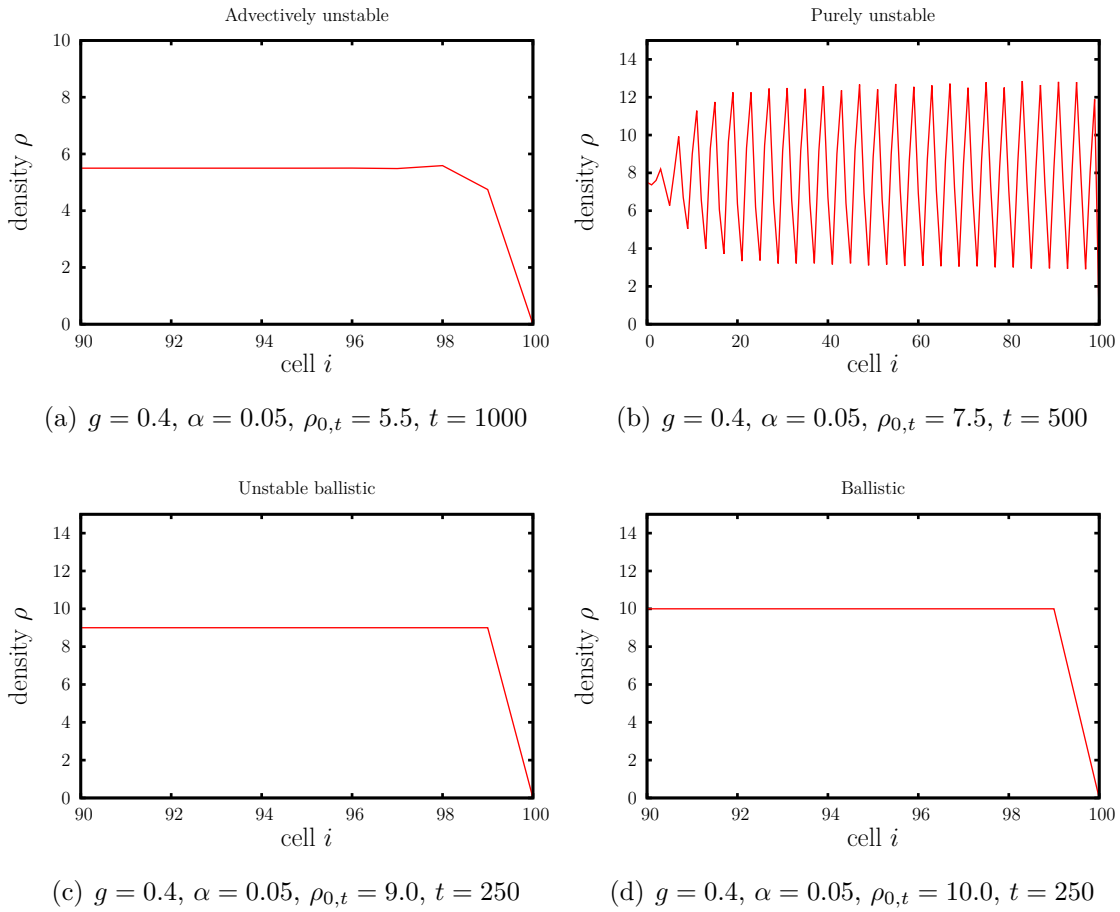

(a) $g = 0.4$, $\alpha = 0.05$, $\rho_{0,t} = 5.5$, $t = 1000$

(b) $g = 0.4$, $\alpha = 0.05$, $\rho_{0,t} = 7.5$, $t = 500$

(c) $g = 0.4$, $\alpha = 0.05$, $\rho_{0,t} = 9.0$, $t = 250$

(d) $g = 0.4$, $\alpha = 0.05$, $\rho_{0,t} = 10.0$, $t = 250$

Figure 4.2.: Distributions after a sufficient time for the four regimes advectively unstable, purely unstable, unstable ballistic and ballistic, respectively. Except for the purely unstable regime, all distributions are in steady states

For the advectively unstable regime Fig. 4.2 (a) we observe a slight increase of the density right before the dip. The purely unstable regime in (b) does not reach an equilibrium state like the one seen in Fig. 3.8. The unstable ballistic regime in (c) and the ballistic regime in (d) look essentially the same, a uniformly distributed density right before a very steep, straight dip. This is obvious, since at this point they are in the same regime. The unstable ballistic regime only exists for nonuniform distributions with some cells containing a density small enough for the cut-off condition not to kick in. The mechanism how unstable behaviour appears in these circumstances is explained in section 3.1.4.

The transition between the diffusive decay and advectively unstable regime is smooth, meaning a definite threshold could not be identified. First we face mostly diffusive behaviour in the diffusive decay regime (see Fig. 4.1). For increasing values of $\alpha\rho$ the dip at the outlet becomes steeper until at some point even a little stationary peak arises right before the outlet (see Fig. 4.2 (a)).
Entering the purely unstable regime, the peak at the outlet starts to grow and produces fluctuations left from it (see Fig. 3.8).

4.2. Analytical approach to equilibrium states of the diffusive decay regime

The steady state density distribution can be calculated analytically by solving the BURGERS equation (2.24) for $\frac{\partial \rho(x,t)}{\partial t} = 0$. Therefore we start from

$$j(x) = C\rho^2(x) - D\frac{\mathrm{d}\rho(x)}{\mathrm{d}x} \tag{4.1}$$

and perform a separation of variables

$$D\frac{\mathrm{d}\rho}{\mathrm{d}x} = C\rho^2(x) - j \tag{4.2}$$

$$\Leftrightarrow \int_x^L \frac{1}{D}\mathrm{d}x = \int_\rho^0 \frac{1}{C\rho^2(x) - j}\mathrm{d}\rho(x) \tag{4.3}$$

$$\frac{1}{D}(L - x) = \int_\rho^0 \frac{1}{C\rho^2(x) - j}\mathrm{d}\rho(x) \quad , \tag{4.4}$$

where $L = m \cdot a$ is the size of our system while we choose $D \neq 0 \neq C\rho^2(x) - j$. Now we substitute

$$z := \rho(x)\sqrt{\frac{C}{j}} \tag{4.5}$$

$$\Rightarrow \rho(x) = z\sqrt{\frac{j}{C}} \tag{4.6}$$

$$d\rho = \sqrt{\frac{j}{C}}\mathrm{d}z \tag{4.7}$$

and get

$$\frac{1}{D}(L-x) = \int_{\sqrt{\frac{j}{C}}z}^{0} \frac{1}{z^2-1}\sqrt{\frac{1}{jC}}\mathrm{d}z \tag{4.8}$$

$$= \tanh^{-1}\left(\sqrt{\frac{j}{C}}z\right) \quad . \tag{4.9}$$

Solving for $\rho(x)$ and resubstituting z, we obtain

$$\rho(x) = \tanh\left(\sqrt{jC}\left(\frac{L-x}{D}\right)\right) \quad . \tag{4.10}$$

To include the inlet boundary condition we divide $\rho(x)$ by the density $\rho(x=0) =: \rho_0$ at the inlet and get

$$\frac{\rho(x)}{\rho_0} = \frac{\tanh\left(\sqrt{jC}\left(\frac{x-L}{D}\right)\right)}{\tanh\left(\sqrt{jC}\left(\frac{L}{D}\right)\right)} \quad . \tag{4.11}$$

We define $\sqrt{\frac{jCL^2}{D^2}} =: k$ and obtain

$$\frac{\rho(x)}{\rho_0} = \frac{\tanh(k(1-\frac{x}{L}))}{\tanh(k)} \quad . \tag{4.12}$$

The Fig. 4.3 plots $\frac{\rho(x)}{\rho_0}$ as a function of k and x.

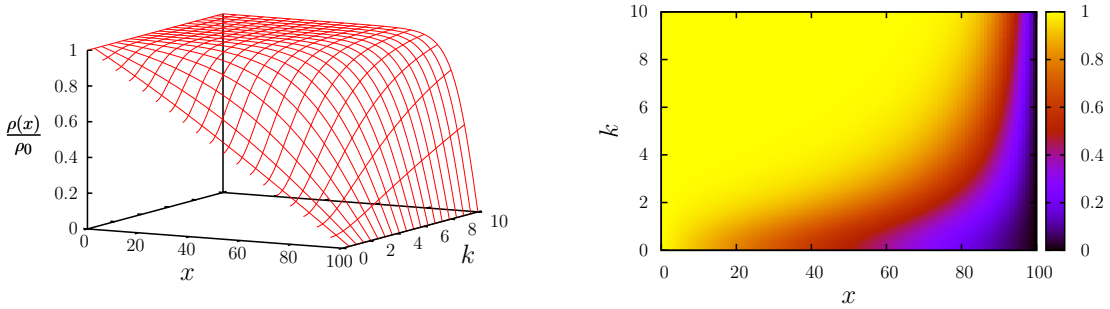

Figure 4.3.: The analytical solution of steady states in the diffusive decay regime like shown in Eq. (4.12).

To compare the solution with numerical results we rewrite Eq. (4.11) as

$$\rho(x) = \frac{\tanh\left(\sqrt{jC}\left(\frac{x-L}{D}\right)\right)}{\tanh\left(\sqrt{jC}\left(\frac{L}{D}\right)\right)} \cdot \rho_0 \tag{4.13}$$

and use the values for C and D defined in Eq. (2.18). In order to find the value of j of a system we wait until the system has reached a steady state and compute the flux at the outlet (outflux). The steady state flux is constant in space and time and therefore equals the outflux. Then for a given inlet boundary condition $\rho_{0,t}$, we use (4.13) to derive the corresponding theoretical curve. In Fig. 4.4 we plot both the theoretical prediction and the numerical solution. Given the perfect overlap, we also plot their difference in the inset of Fig. 4.4.

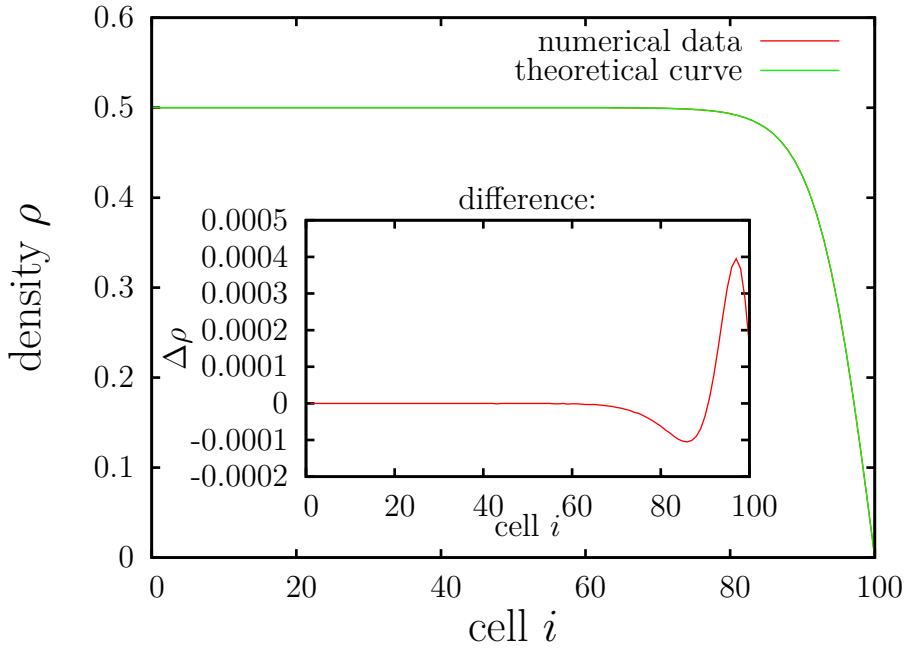

Figure 4.4.: A steady state for $g = 0.4$, $\rho_{0,t} = 0.5$, $\alpha = 0.05$ and its analytical solution for $a = 1$, $\tau = 1$ and therefore $C = 2\alpha = 0.1$, $D = g = 0.4$, $m = 100$, $j = 0.025$, $\rho_0 = \rho_{0,t} = 0.5$. Inset figure: A plot of the difference in the density $\rho_{numerical} - \rho_{theoretical}$ versus the cells i.

The fit between the two curves is very good except for the absorbing boundary. As shown in Fig. 4.2, at the outlet a small increase of the density arises when entering the advectively unstable regime. At this point, the analytical solution stops

applying. Therefore, we can say that it is in good agreement with the simulated data for the diffusive decay regime. The mismatch of the analytical solution and the numerical data at the absorbing edge was to be expected, since the BURGERS equation does not include absorbing boundaries.
Also the analytical solution does not incorporate any instabilities. Therefore it will not match the numerical data the closer we are to the purely unstable regime.

4.3. Discussion

We observed, that equilibrium distributions depend only on the boundary conditions, as far as there exist equilibrium distributions. For the purely unstable regime we observed a spiky distribution instead.
The analytical determination of the equilibrium distribution in the diffusive decay regime and its comparison with numerical results was originally supposed to verify our model, but it also provides valuable results. As shown in Fig. 4.4 over the first 70 cells the theory is in excellent agreement with our numerical data. Although we see differences at the last 30 cells, the consistency is still amazing since the differences are small.

5. Non-equilibrium phase transitions

In this section we analyze the location of each regime dependent on the parameters α, g, $\rho_{0,t}$ and γ and then creating phase diagrams. With this we will determine the location of the transitions, try to analytically predict them and explain their existence.
To this end we will first introduce cumulative density functions (cdfs) as well as explain how we can use them to determine the regime in which a certain system lives. Then we introduce *cdfwidth* plots which essentially are phase diagrams showing the location of regimes. Phase diagrams created with constant influx allow us to determine the parameters leading to the purely unstable regime in section 5.3. For noisy influx in section 5.4 we then are able to identify the other regimes as well.

5.1. Introduction of cdfs

Our main interest is to determine the location of each regime. Therefore we investigate the dependence of the fluid moving from cell $i = m - 1$ to cell $i = m$ and therefore leaving the system ρ_{out} as a function of $\rho_{0,t}$, α, g and γ.
To prevent influence of the initial density distribution, we wait until the system reaches a steady state. We then construct the cdf of the outflux. A sketch of the following steps:

1. Pick fixed values for $\rho_{0,t}$, α, g , m and γ.
2. Run the simulation until the density distribution reaches steady state.
3. Calculate the fluid jumping from cell $i = m - 1$ to $i = m$ at each time step, i.e. the amount of fluid leaving the system per time-step. We usually collect 5000 values between $t = 10000$ and $t = 20000$.
4. Sort the values in increasing order and number them. Then normalize to 1.

5. `Plot the normalized numbers versus the fluid density leaving the system` ρ_{out}.

Figure 5.1 (a) shows the cdf for the diffusive decay regime with white noise of amplitude $\gamma = 1.0$.

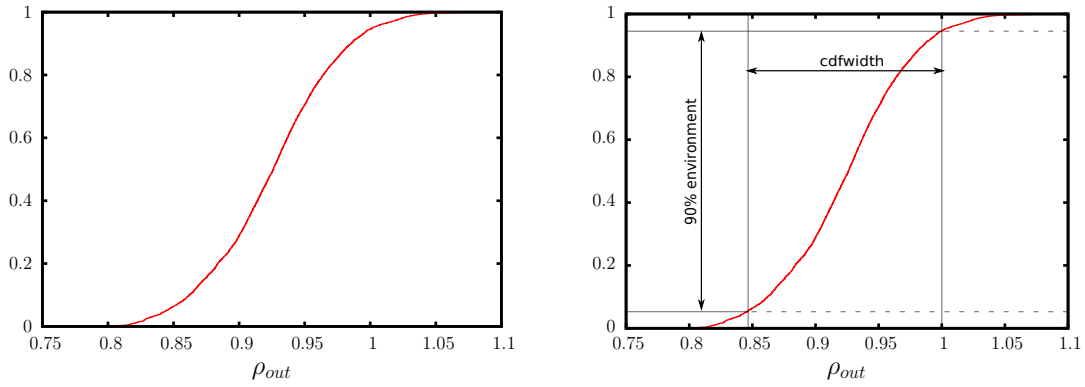

(a) (b)

Figure 5.1.: (a) shows a cdf for the diffusive decay regime. We used $n = 5000$ values, every second value starting from time-step $t = 10000$. (b) shows how to measure the 90% width of such cdf. Parameters: $\alpha = 0.05$, $g = 0.4$, $\rho_{0,t} = 3.0$, $\gamma = 1.0$.

The cdf describes the probability that the amount of fluid leaving the system per time-step is less than or equal to ρ_{out}. For instance when we look at the outflux $\rho_{out} = 0.9$, the corresponding value on the y-axis is ≈ 0.3. Thus we can assume that around 30% of all matter flowing out per time-step is smaller than $\rho_{out} = 0.9$. Furthermore we can identify the area which contains 90% of all ρ_{out} values. This corresponds to a 1.64σ deviation of the average as shown in Fig. 5.1 (b).

For now we only consider deterministic systems, so we will have no noise in the influx if not explicitly mentioned. The cdf for the same set of parameters and no noise is given in Fig. 5.2.

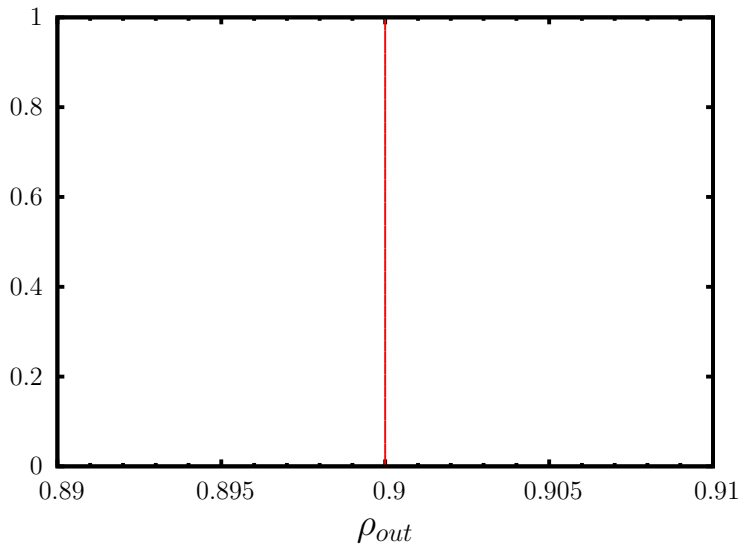

Figure 5.2.: A cdf for the diffusive decay regime. We used $n = 5000$ values, every second value starting from time-step $t = 10000$ with $\alpha = 0.05$, $g = 0.4$, $\rho_{0,t} = 3.0$,$\gamma = 0$.

The step function observed in Fig. 5.2 is what we expected: in the steady state diffusive regime since the influx is constant, the outflux is constant and there are no fluctuations in the density. This leads to a step function cdf.
The behaviour drastically changes when the purely unstable regime is reached as shown in Fig. 3.8. There, spikes grow at the outlet and no equilibrium state is reached. Therefore the spectrum of the amount of fluid leaving the system is obviously very broad. The following figure shows a cdf for such a regime:

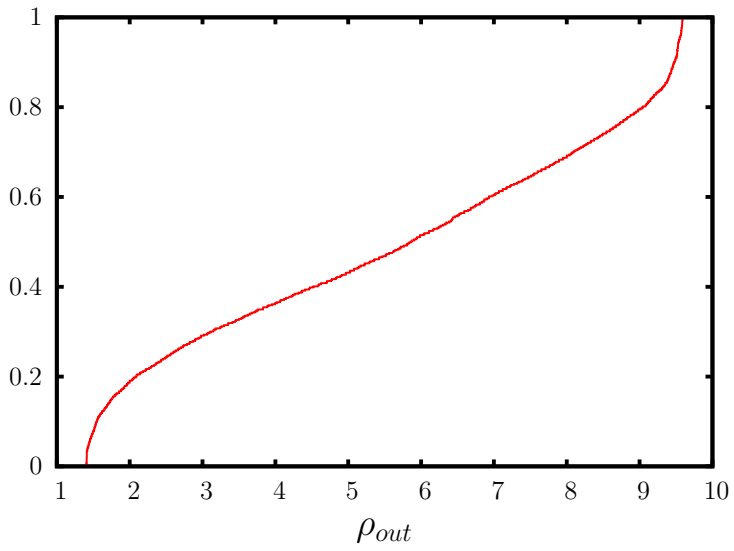

Figure 5.3.: A cdf for the purely unstable regime. We used $n = 5000$ values, every second value starting from time-step $t = 10000$ with $\alpha = 0.05$, $g = 0.4$, $\rho_{0,t} = 7.5$, no noise($\gamma = 0$).

The outflux explores values from around $\rho_{out} \approx 0.5$ to $\rho_{out} \approx 9.5$ leading to a very broad cdf. Since every regime except the purely unstable regime ends up in a steady state after large times, their cdfs then look like the one in the diffusive decay regime in Fig. 5.2, only with the appropriate value for the average of outflux. However, since there is no such steady state for the purely unstable regime, its cdf will never be step-function-like.

5.2. Introduction to cdfwidth plots

Section 5.1 leads us to make the assumption that the regime in which the system develops can be fully identified by the width of its cdf which we will refer to as *cdfwidth*. Our *cdfwidth* is chosen to correspond to the 90% interval:

$$\text{cdfwidth} := \text{quantile}_{95\%} - \text{quantile}_{5\%} \quad . \tag{5.1}$$

A $\text{quantile}_{x\%}$ marks the outflux $\rho_{out,x}$ for which $x\%$ of the values ρ_{out} are smaller than or equal to $\rho_{out,x}$.

A plot of the *cdfwidth* as a function of $\rho_{0,t}$ and α (with constant $g = 0.4$ and no noise($\gamma = 0$)) looks as follows:

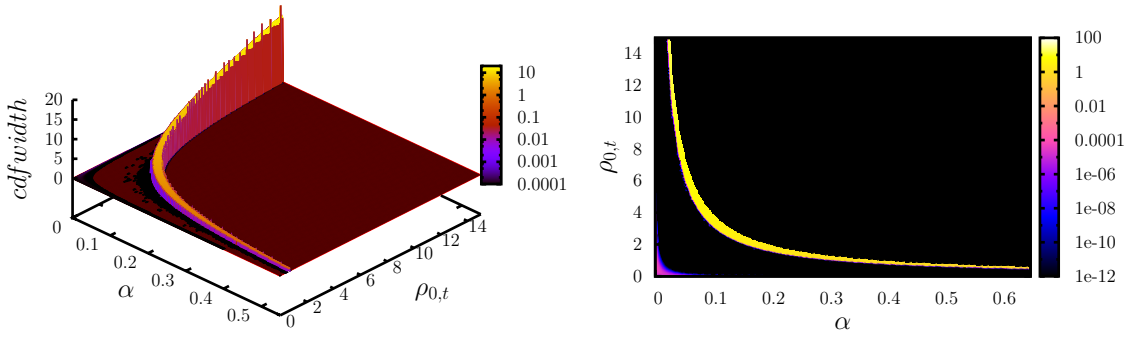

(a) (b)

Figure 5.4.: A plot of the 90% width of a cdf versus its parameters $\rho_{0,t}$ and α for constant $g = 0.4$ and no noise($\gamma = 0$). (a) shows it as 3d plots whereas (b) shows a 2d false color plot.

In (a) we see most values for the *cdfwidth* are equal to zero, except one curve whose height reaches *cdfwidth* ≈ 20 for low values of α and large values of $\rho_{0,t}$, and *cdfwidth* ≈ 1 for large values of α and small values of ρ. We can identify the curve as the purely unstable regime due to our previous observation of Fig. 5.2. In (b) a two-dimensional false color plot is given where we see the top view of (a) with the *cdfwidth* determined by color. Our observations in section 3.1 imply, that the violet and black area in the bottom left corner contains the diffusive decay as well as the advectively unstable regimes. Also the observations imply the black area in the top right contain the unstable ballistic and the ballistic regimes. The yellow area contains the purely unstable regime, since we face cdfs with certain width$\neq 0$.
The purple area (larger view in Fig. 5.5) originates from initial density fluctuations left in the system. In this area $t = 10000$ time-steps are not enough time for the initial density distribution to vanish completely. The minimum time required for the system to reach steady state is controlled by the slower transport process (i.e. diffusion or advection). Therefore, the steady state is reached after a time $t \geq \max\{T_D, T_v\}$, where $T_D = \frac{m^2}{D}$ and $T_v = \frac{m}{v} = \frac{m}{C\rho}$ are the typical timescales associated with diffusive or advective transport, respectively. C and D are given by Eq. (2.18).

The time for a distribution to vanish completely by diffusion or advection, is shown in Fig. 5.6.

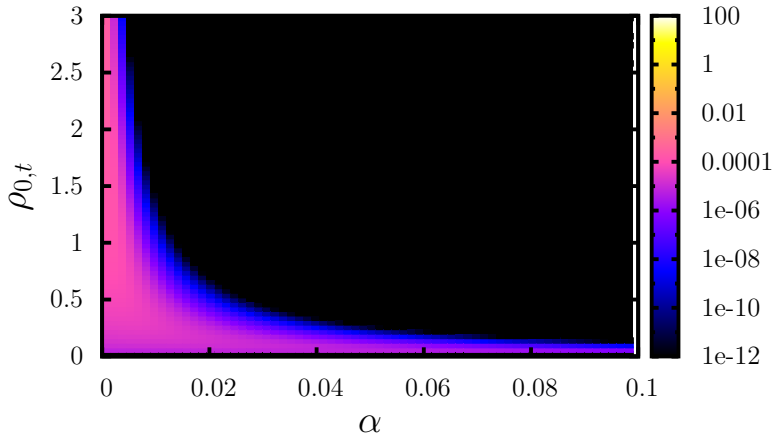

Figure 5.5.: A plot of the 90% width of a cdf versus its parameters $\rho_{0,t}$ and α for constant $g = 0.4$ and no noise($\gamma = 0$) as map. (A blow-up of the purple area in the bottom left corner of Fig. 5.4 (b))

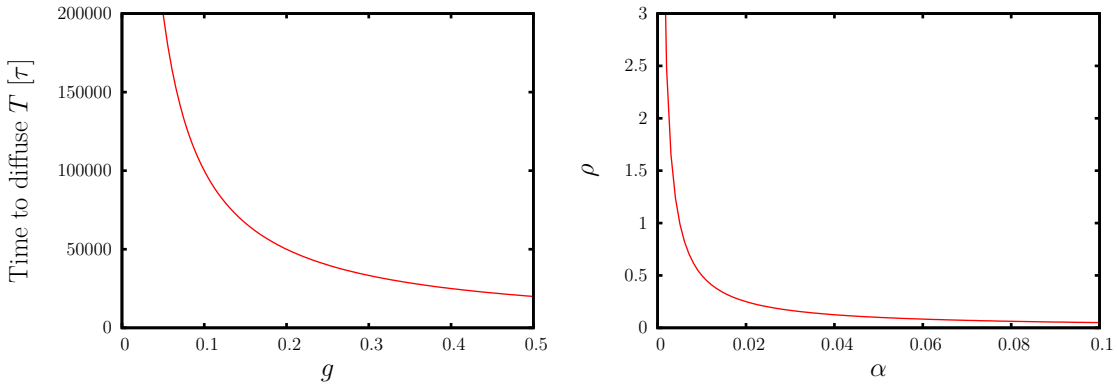

Figure 5.6.: (a) shows the time until a system of size $m = 100$ completely vanishes by diffusion. (b) shows the values of ρ and α where a system vanishes purely by advection during 10000τ

In (a), we can see that it takes a distribution at least 20000 time-steps to vanish purely by diffusion. The curve in (b) shows the values of ρ and α which are necessary for a distribution to vanish purely by advection during $t = 10000$ time-steps. The curve fits approximately the transition area between purple and black in Fig. 5.5. Thereby we learn, initial distributions for systems with parameters in the purple area need more than 10000 time-steps in order to reach a steady state. Anyway, the values of $cdfwidth$ there will turn to $cdfwidth = 0$ for sufficiently large times.

5.3. Phase diagrams for constant influx

We now want to analyze the impact of values of g on the width of a cdf and thus learn about the impact of g on the location of the purely unstable regime. In the following figure we show phase diagrams for different values of g:

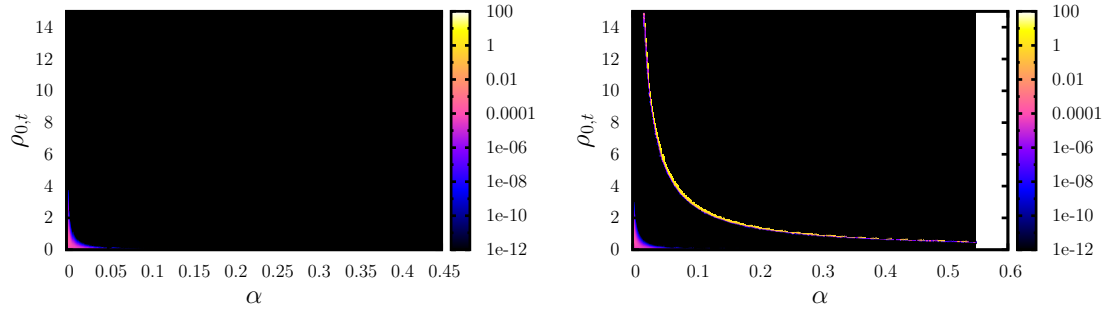

(a) $g = 0.2$ (b) $g = 0.3$

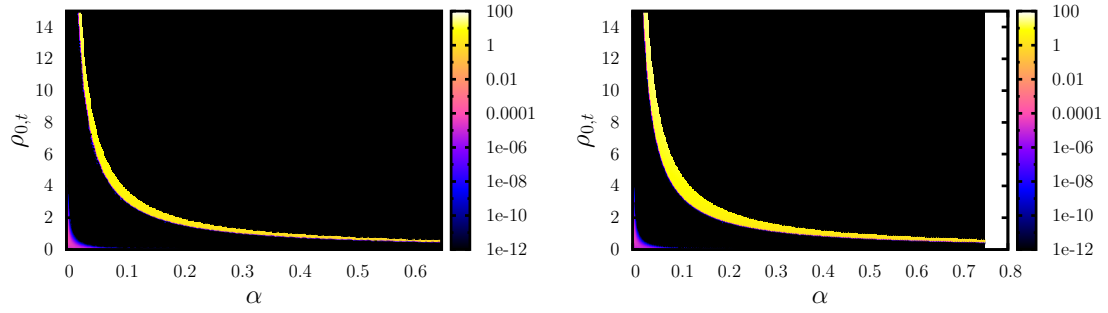

(c) $g = 0.4$ (d) $g = 0.5$

Figure 5.7.: Phase diagrams for different values of g, no noise($\gamma = 0$).

The general shape of the purely unstable regime area stays the same, but we recognize that the curve is broadening for higher values of g. Also for $g = 0.2$ we see no unstable regime at all.

Now we try to analytically approximate the borders of the purely unstable regime. Since a characteristic of the ballistic regime is to have no probability to jump left anymore, we can assume the upper boundary of the purely unstable regime is given by $l_i = g - \alpha\rho = 0$. Thereby we obtain $\rho_{u.b.} = \frac{g}{\alpha} =: \frac{g_{u.b.}}{\alpha}$ as a function for the upper border and compare it to the contours of the purely unstable regime. The following figure shows the contours of the purely unstable regime from Fig. 5.7 (b) and (d), each with its analytical upper border:

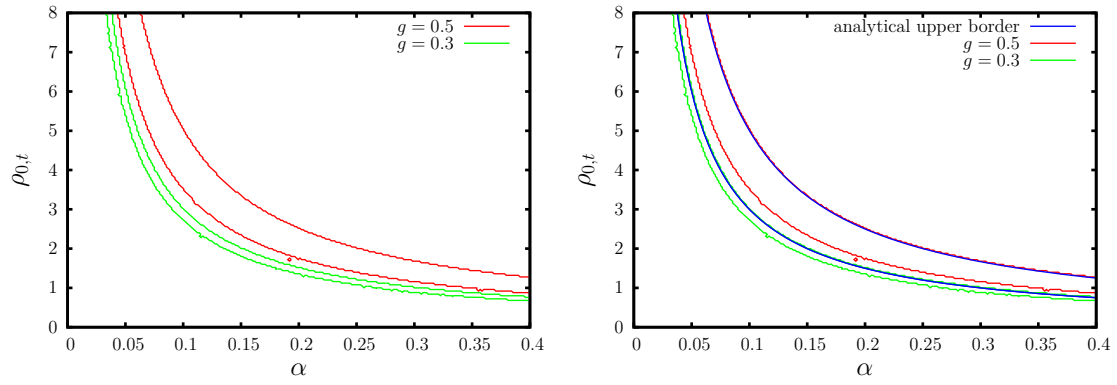

(a) (b)

Figure 5.8.: The contours of the purely unstable regimes of Fig. 5.7 created with the values at height $cdfwidth = 0.01$. In (b) an analytical solution is shown additionally, for $g = 0.5$: $\rho_{u.b.,g=0.5} = \frac{0.5}{\alpha}$; for $g = 0.3$: $\rho_{u.b.,g=0.3} = \frac{0.3}{\alpha}$.

The approximation fits the upper borders quite well. Also, we recognize that the purely unstable regime not only shrinks for greater values of g, it also moves closer to the origin. Furthermore we can assume the borders of one purely unstable regime will collide for a small enough value of g, since in Fig. 5.7 (a) no purely unstable regime is visible anymore.

Assuming, the lower boundaries follow the same behaviour as the upper borders $\rho_{l.b.} = \frac{g_{l.b.}}{\alpha}$, we made a fit of the lower borders of the purely unstable regime in Fig. 5.7 (b) to (d) and obtained values for $g_{l.b.}$. In Fig. 5.9 the results for 5.7 (b) and (d) are illustrated.

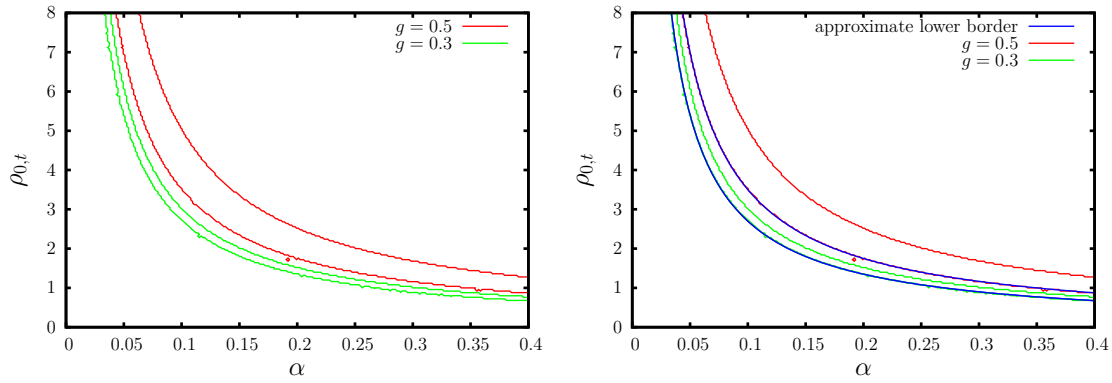

(a) Contours of the unstable regimes at height $cdfwidth = 0.01$

(b) Contours with analytical curves of the lower borders

Figure 5.9.: The contours of the purely unstable regimes of the phase diagrams 5.7 (b) and (d) and their lower border fits. For (b) with $g = 0.3$ we obtained $g_{l.b.} = 0.27$, for (d) with $g = 0.5$ we obtained $g_{l.b.} = 0.35$. The map in Fig. 5.7 (c) for $g = 0.4$ is not illustrated but goes with $g_{l.b.} = 0.31$. The according functions are of the form $\rho_{l.b.} = \frac{g_{l.b.}}{\alpha}$.

We can confirm the lower border follows the same type of function as the upper border.

Now to determine at which point the curves intersect and thereby the unstable system disappears, we extrapolate the obtained values for $g_{l.b.}$. The following figure shows the values of $g_{l.b.}$ versus $g_{u.b.} = g$:

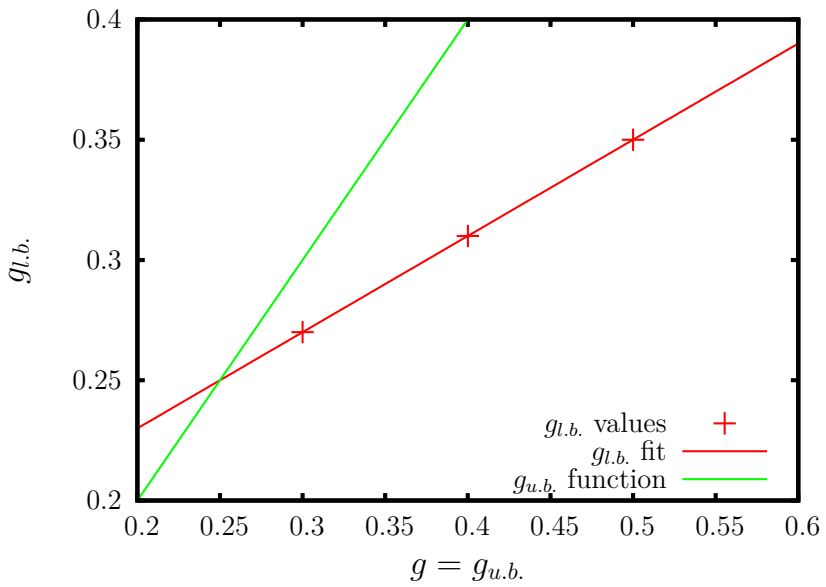

Figure 5.10.: The approximated values for $g_{l,b}$ with a fit (red) and our theoretical function for values of $g_{u.b}$ (green).

We see that the approximated function of $g_{l.b.}$ fits perfectly and crosses the function of $g_{u.b.}$. The point in which they cross is given by

$$g_{cross} = 0.4 \cdot g_{cross} + 0.15 \tag{5.2}$$

$$\Rightarrow g_{cross} = 0.25 \quad . \tag{5.3}$$

For $g = 0.25$ the upper border and the lower border are identical and thereby the purely unstable system does not exist for any value of $g \leq 0.25$.

5.4. Phase diagrams for noisy influx

From the previous section we learned how to determine the parameters leading to a system in the purely unstable regime. But still we can not distinguish between the unstable ballistic and the ballistic regime. And since the transition from the diffusive decay to the advectively unstable regime is smooth, we generally cannot distinguish between them either.
In this section we try to distinguish between regimes which dissolve and regimes which explode by adding a random noise to the influx. The regimes with growing

behaviour will now appear at *cdfwidth* plots since spikes broaden the cdf of a system. The following figure shows a *cdfwidth*-map for $g = 0.4$ and a white noise of amplitude $\gamma = 0.5$:

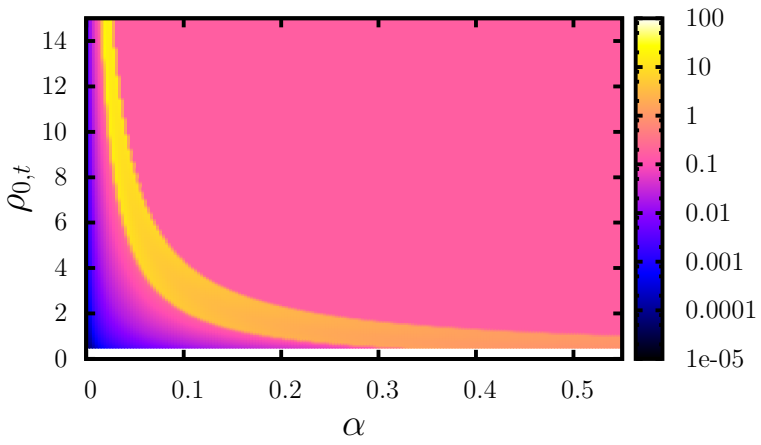

Figure 5.11.: A plot of the *cdfwidth* versus its parameters $\rho_{0,t}$ and α for constant $g = 0.4$ and $\gamma = 0.5$ as map.

We see a yellow area shaped like the unstable area in the plots for deterministic systems. Also we see no points with $cdfwidth = 0$ anymore.
The yellow area now contains the unstable regime as well as parts of the advectively unstable and the unstable ballistic regime, since now spikes can evolve out of the random influx. In the ballistic regime, the value of the width is close to the value of the white noise. Since in the ballistic regime the advection is at its maximum, the fluctuations in the density caused by the white noise have little time to smooth out. Therefore the density flowing out of the system varies with a magnitude of the order of the white noise.
In the diffusive decay and the advectively unstable regime (which we can not really distinguish) we observe a smooth transition in *cdfwidth*. The advection grows for higher values of ρ and α as the time for a peak to diffuse shrinks. At some point, peaks do not dissolve anymore and finally start growing. However, for $m \to \infty$ and $t \to \infty$ we would observe sharp transitions.
The small bar of missing data from $\rho = 0.0$ to $\rho = 0.5$ is unavoidable, since with a white noise of amplitude $\gamma = 0.5$ we could have negative values of the density for

any initial density lower than $\rho_{0,t} < 0.5$.
We now compare *cdfwidth* maps for different values of γ:

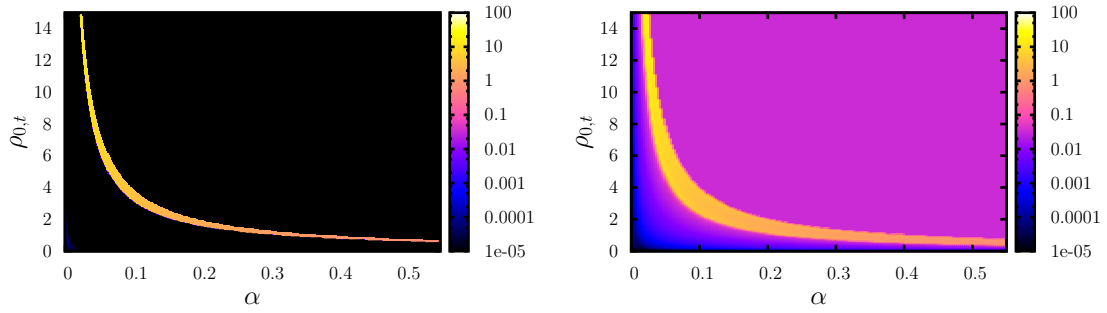

(a) $\gamma = 0.0$ (b) $\gamma = 0.1$

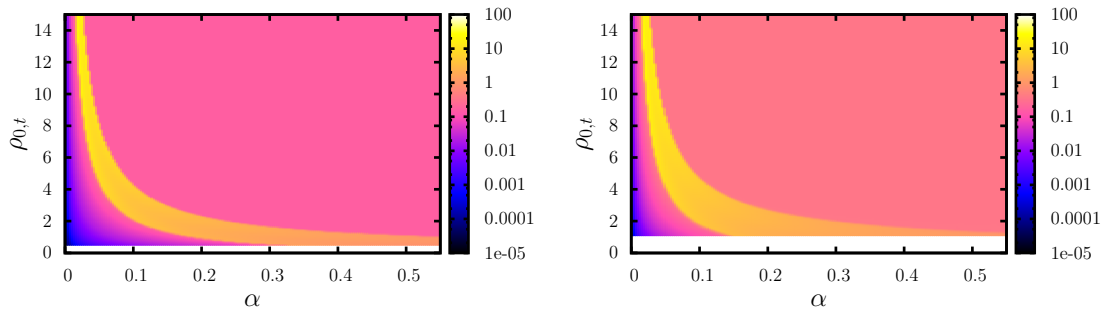

(c) $\gamma = 0.5$ (d) $\gamma = 1.1$

Figure 5.12.: Phase diagrams for different values of γ with constant $g = 0.4$.

For stronger white noises the unstable regime grows in width and the ballistic regime has larger *cdfwidth*s. The broader yellow area for larger values of γ has several reasons. For the advectively unstable regime: In general, the greater a peak, the faster it grows like seen in Fig. 3.15. So some peaks which normally would not grow significantly high before leaving the system suddenly do so, as long as the white noise amplitude and therefore the initial height of a peak is large enough. For the unstable ballistic regime: With wider distributed densities more spikes reach into the unstable regime and therefore cause a growth like described in section 3.1.4.
The upper border of the yellow curves in Fig. 5.12 can be easily approximated. We use the same condition of $l_i = 0$ for the transition just like in the deterministic

case. Only now, since the white noise adds fluctuations which can reach the unstable regime we simply map $\rho \to \rho - \gamma$. Thereby we get

$$\begin{aligned} l_i = 0 &= g - \alpha(\rho - \gamma) \\ \Leftrightarrow \rho &= \frac{g}{\alpha} + \gamma \quad , \end{aligned} \tag{5.4}$$

which fits the numerical data:

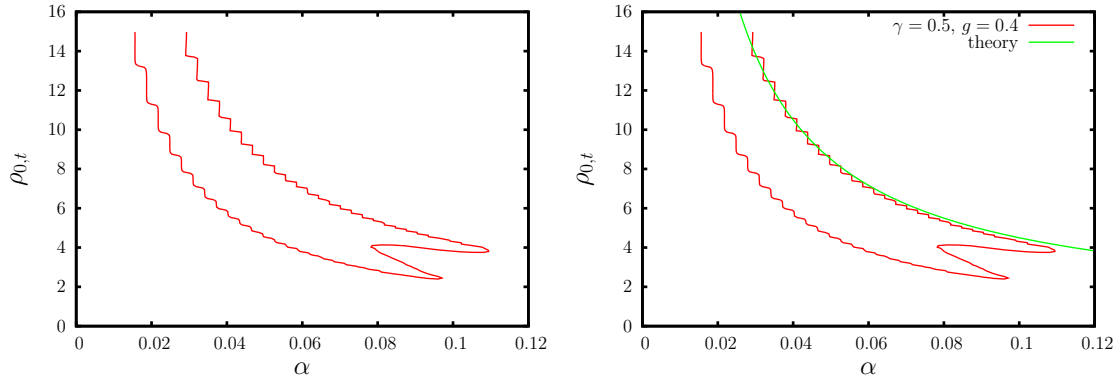

(a) (b)

Figure 5.13.: The contours of a phase diagram with $\gamma = 0.5$, $g = 0.4$, created with the values at height $cdfwidth = 5.0$. In (b) an analytical solution is shown on top of the data.

The contours were created by all values of height $cdfwidth = 5.0$ and therefore the lower border is not meaningful since the transition between the diffusive decay and the advectively unstable regime is smooth.

5.5. Discussion

We now can both determine the purely unstable regime, as well as give a good approximation of the unstable ballistic and the advectively unstable regime numerically for any parameters. We are even able to analytically determine the borders of the purely unstable regime. We learned that for $g < 0.25$ the purely unstable regime does not exist (see Fig. 5.10). The upper border is determined by $\rho(\alpha) = \frac{g}{\alpha}$, whereas the lower border was determined to be of the same shape. For constant influx we were able to approximate a function to fit the lower border, while for noisy

influx no sharp lower border appeared. For infinite time and an infinite size of the system we would be able to see one, though.
The unstable ballistic and the ballistic regime are essentially identical, only in the unstable ballistic regime the density at some cells is small enough to create a probability to jump left of $l_i > 0$. Thus, peaks can arise as described in section 3.1.4. Still, for a noise with amplitude γ in the influx, we were able to determine the transition as $\rho(\alpha) = \frac{g}{\alpha} + \gamma$.
If we actually choose values for g and α such that $g \gg \alpha$ (as mentioned in section 2.1), i.e. $\alpha \leq 0.01$, we observe the system to be in the diffusive decay regime even for very large densities (as shown in Fig. 5.11).

6. Conclusion & Outlook

We have used a biased random walk to numerically model the spatial and temporal distribution of water density in soil. As shown in section 2.2, in the continuum limit our model corresponds to the one-dimensional BURGERS equation. The probabilities to jump were defined in section 2.1 as follows:

$$r_{i,t} = g + \alpha\rho_{i,t} \tag{6.1}$$

$$l_{i,t} = g - \alpha\rho_{i,t} \tag{6.2}$$

$$s_{i,t} = 2g \quad , \tag{6.3}$$

where we could identify g and α in section 3.1.1 to determine the diffusive and the advective behaviour of a system, respectively. In section 3 and 4 we were able to identify five different regimes which differ in behaviour. There we used mostly the same values for the parameters g, α and m, only the average density of the system combined with the constant influx $\rho_{0,t} = A$ were increased from very small values, until the behaviour would not change anymore.

1. The **diffusive decay regime** provided us with diffusive and slightly advective behaviour.

2. In the **advectively unstable regime**, which branched out of the diffusive decay regime when fluctuations in the density grow instead of diffuse. Still the whole density distribution advected to the outlet thereby leaving the system to reach steady state.

3. The **purely unstable regime** behaved like the advectively unstable regime, only now no steady state was ever reached. Spikes evolved out of irregularities in the density distribution and were able to spread out upstream.

4. This behaviour ended in the **unstable ballistic regime** once the advection was strong enough to "wash out" the spikes. Still spikes showed up but now by a different mechanism which was described in detail in section 3.1.4.

5. No more growing but a highly advective behaviour was observed in the **ballistic regime**. In this regime, the probability to jump left $l_{i,t}$ is zero. For higher densities the behaviour does not change since the cut-off condition from Eq. (2.8) keeps the jump probabilities fixed preventing them from taking negative values.

In order to simulate a daily or hourly variation in precipitation we added a random noise to the influx. In the diffusive decay regime it only had a small impact on the outflux and the general evolution since the noise quickly diffused. In the other regimes however the noise lead to huge differences since either it grew into spikes or it advected quickly through the system diffusing just a little.
In section 4 we analyzed the equilibrium distributions of each regime and found an analytical solution for the steady states in the diffusive decay regime. This solution is in excellent agreement with our numerical results, therefore verifying our model (see Fig. 4.4).

In order to predict the behaviour of a system with a fixed set of parameters g, α, $\rho_{0,t}$ and m, in section 5 we constructed phase diagrams which allowed us to determine the regime for every set of parameters.
We first looked at the amount of fluid leaving the system for a steady state and deterministic boundary conditions and created a cdf of it. By plotting the width of the cdf versus α and $\rho_{0,t}$ we were able to determine the values for parameters which lead to the purely unstable regime. The only system with fluctuations in the outflux (for constant influx) is the purely unstable regime, which is therefore the only regime we observe in Fig. 6.1 (a). When we added a random noise to the influx, no steady state can be reached but still the initial distribution vanishes. With noisy influx also the advectively unstable, as well as the unstable ballistic regime, became visible in the phase diagrams. Thereby we could estimate the parameters which correspond to each system. In Fig. 6.1 two phase diagrams are shown, (a) without and (b) with random noise in the influx.

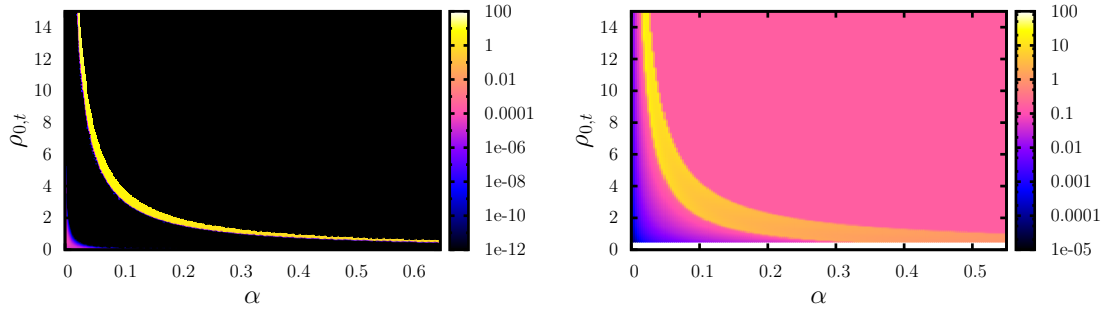

(a) $g = 0.4$, $\gamma = 0.0$

(b) $g = 0.4$, $\gamma = 0.5$

Figure 6.1.: A phase diagram with and without white noise added to influx. In (a) we see the purely unstable regime as a yellow area. In (b) we can determine the rate of disturbances in the density growing. Thereby we can estimate the area of the advectively unstable and the unstable ballistic regime. To learn about the approximate location of all five regimes, we have to look at both plots (a) and (b), since the purely unstable regime is not explicitly visible in (b).

Some transitions between two regimes were analytically provided in section 5. Since the transition from diffusive decay to advectively unstable is smooth we were not able to determine a clear border. Still, for a very large system and very long time we could determine the border when peaks start growing.

The transition between the advectively unstable and purely unstable regime was approximated in section 5.3. We found an approximated function by adjusting the border between the purely unstable and the unstable ballistic regime. We determined this border by identifying the unstable ballistic regime to generally move at maximum speed since the cut-off condition from Eq. (2.8) kicks in. Therefore we determined the border to be $\rho(\alpha) = \dfrac{g}{\alpha}$.

The unstable ballistic and the ballistic regime are essentially the same. When the density at some cells is low enough to create a probability to jump $l_i > 0$, peaks can grow like described in section 3.1.4. However, for a noisy of amplitude γ in the influx the border is determined by $\rho(\alpha) = \frac{g}{\alpha} + \gamma$.

So, what did we learn? Our model produces higher advection for a larger amount of fluid. Therefore it could qualitatively describe the evolution of water from a catchment area to a river, ergo evolution of water in large scale soil. We were able to observe transients of different initial distributions in section 3 and analyze the impact of random precipitation patterns simulated by a noisy in the influx. It turned out, that the noise either diffused quickly in the diffusive decay regime, or grew into spikes. In the ballistic regime the noise rushed downstream. The only significant difference was, that the white noise prevented the system from reaching an equilibrium state in the unstable advective and the purely unstable ballistic regime.
Unfortunately the flower pot could not be found in any part of our model. However, to model such system we could choose different probabilities to jump, like for example

$$r_{i,t} = g + \alpha \exp(-c\rho_{i,t}) \quad , \tag{6.4}$$

$$l_{i,t} = g - \alpha \exp(-c\rho_{i,t}) \quad , \tag{6.5}$$

with constant c. Now, for low densities the advection becomes stronger whereas for very large densities it becomes purely diffusive.

Future work will also include the study of the impact of oscillatory boundary conditions

- to simulate variations in precipitation on a seasonal scale,
- to determine the impact of the system parameters on the outflux,
- and to derive its cdfs.

This will allow us to establish the impact of each parameter on the occurrence of rare events, e.g. flooding, for which the full distribution is needed.
Constructing a two-dimensional model will be a natural step to generalize the proposed approach. This will allow modeling more complex systems. Also, subsurface heterogeneity could be incorporated by inhomogeneous jump probabilities, while spatially distributed boundary conditions could be used to describe (spatially) inhomogeneous precipitation patterns.

A. Numerical algorithm

This algorithm was implemented in C and evaluated with gnuplot. It was verified by comparing numerical data with an analytical solution in section 4.2.
At time-step t the algorithm can be formulated as follows:

(1) `Calculate jump probabilities.` For each cell the amount of fluid jumping to the left, jumping to the right or staying at a particular cell i is calculated by using Eqs. (2.9)-(2.11).

(2) `Calculate new densities.` By using the jump probabilities and the density distribution $\rho_{i,t}$, we calculate the density at time-step $t+1$ from Eq. (2.1).

(3) `Apply boundary conditions.` Eq. 2.1 needs to be appropriately modified at the boundaries to account for the missing neighbouring cells. The density of the first cell is set to a value fixed by the inlet boundary condition (see section 2.1). The last cell density is set to $\rho_{m,t+1} = 0$.

(4) `Apply changes in the density.` The new density distribution $\rho_{i,t+1}$ can now be computed by the values obtained in the previous time-step. (Illustrated as sketch in Fig. A.1)

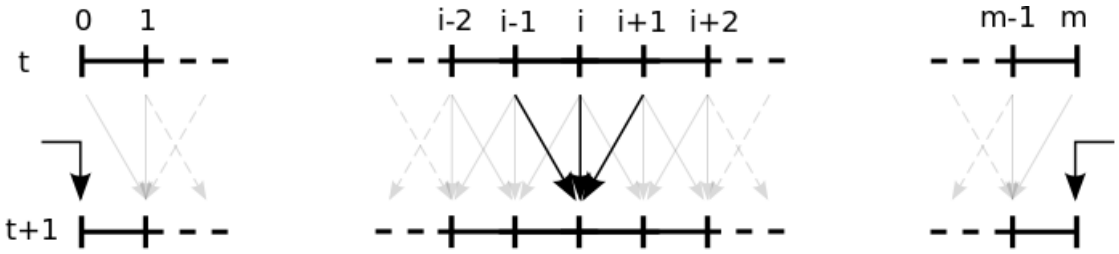

Figure A.1.: Marching the density from time-step t to $t+1$. The arrows indicate fluid moving to the particular cell while the density in the first and last cells is imposed by the boundary conditions.

Bibliography

[1] Ilenia Battiato. Non-linear model for catchment-scale discharge response. (unpublished).

[2] Kevin J. McGuire and Jeffrey J. McDonnell. A review and evaluation of catchment transit time modeling. *Journal of Hydrology*, 330:543–563, 2006.

[3] Kevin E. Trenberth, Aiguo Dai, Roy M. Rasmussen, and David B. Parsons. The changing character of precipitation. *BAMS*, September:1205–1217, 2003.

[4] Jürgen Vollmer. Chaos, spatial extension, transport, and non-equilibrium thermodynamics. *Physics Reports*, 372:131–267, 2002.

[5] Arthur Wachtel. Non-linear response of water flux through a soil column. Bachelors thesis, Max Planck Institute for Dynamics and Self-Organization, 2009.

[6] Guojie Wang, Tong Jiang, Richard Blender, and Klaus Fraedrich. Yangtze 1/f discharge variability and the interacting river-lake system. *Journal of Hydrology*, 351:230–237, 2008.

[7] A. W. Warrick and Gary W. Parkin. Analytical solution for one-dimensional drainage: Burger's and simplified forms. *Water resources research*, 31:2891–2894, 1995.

Acknowledgments

I would like to express my gratitude to all people who helped me creating this thesis. Special thanks is provided for my professor Jürgen Vollmer who helped me with all problems I had to face during the last weeks. The all-night sessions working on the thesis (even right before his vacation) were really fruitful and will not be forgotten.
I thank my supervisor Ilenia Battiato who helped me with the basics of writing a thesis.
I also extend my sincere thanks to Ariane Papke who always had a sympathetic ear and was good company the whole time. Even at last when she was working far away in america, she helped me a lot with gnuplot, LaTeX, and proofreading my thesis.
Furthermore I thank Jan-Hendrik Trösemeier for proofreading and giving good ideas.
I also thank Johannes Blaschke who helped me with his linguistic skills while going through this work.

Erklärung nach §13(8) der Prüfungsordnung für den Bachelor-Studiengang Physik und den Master-Studiengang Physik an der Universität Göttingen:

Hiermit erkläre ich, dass ich diese Abschlussarbeit selbständig verfasst habe, keine anderen als die angegebenen Quellen und Hilfsmittel benutzt habe und alle Stellen, die wörtlich oder sinngemäß aus veröffentlichten Schriften entnommen wurden, als solche kenntlich gemacht habe.
Darüberhinaus erkläre ich, dass diese Abschlussarbeit nicht, auch nicht auszugsweise, im Rahmen einer nichtbestandenen Prüfung an dieser oder einer anderen Hochschule eingereicht wurde.

Göttingen, den 4. Juli 2011

(Hannes Hornischer)